The Potential Use of Degradable Starch Microspheres as a Carrier for Nasal Drug Administration

Degree Project in Pharmaceutical Technology,
2023 Department of Food Technology,
Engineering and Nutrition Lund University
Sweden

30 ECTS credits

Author: Rojda Unal
Supervisors: Kyrre Thalberg
Assistenten supervisors: Emelie Haettner and Thomas Larsson
Examiner: Marie Wahlgren

Acknowledgement

During the spring of 2023, the project was conducted in Lund at Magle Chemoswed, Emmace, and Department of Food Technology, Engineering and Nutrition at Lund University. I want to convey my gratitude for being given the opportunity to work on this exciting and rewarding project.

I am truly thankful for the support and assistance provided by my co-supervisors, Emelie Haettner and Thomas Larsson, throughout the project. I also want to thank my supervisor, Kyrre Thalberg, for his help and guidance, and Marie Wahlgren, for being my examiner at Lund University.

Lastly, I want to convey my gratitude to Lars-Erik Briggner, Peter Elfman, and all Magle Chemoswed and Emmace workers who provided access to equipment and assistance during the laboratory parts.

Abstract

Intranasal drug delivery is a practical and accessible method for treating localized symptoms as well as achieving systemic drug absorption. The approach takes advantage of the permeability, vascularization, and limited enzymatic activity of nasal tissue, leading to enhanced drug absorption. Moreover, drugs can bypass the blood-brain barrier and directly reach the brain through the olfactory route. Nasal powder formulations present advantages over liquids, including improved mucosal clearance resistance, simplified composition, larger administration doses, and improved formulation stability. In this study, four different types of degradable starch microspheres (DSM), namely DSM-A, DSM-S, DSM-T, and DSM-L were evaluated for their potential use as nasal drug formulations. Furthermore, the microspheres were combined with a breath-actuated powder inhaler, ICOone Nasal. Initially, the physicochemical characteristics of the DSM batches were assessed, followed by performance testing, where they were loaded into the device to investigate their delivery performance. Additionally, nasal deposition studies were conducted using a 3D-printed nasal cavity model.

The results revealed that, among the DSM batches, DSM-A is the most favorable option for nasal drug delivery, while DSM-S is the least preferred. DSM-A consists of easily dispersible particles not prone to agglomeration, distinguishing it from the other batches, particularly DSM-S, which exhibits high cohesive properties. In dry storage conditions, all batches exhibit excellent flow properties. DSM-A demonstrates the highest flowability, while DSM-S shows the poorest resulting in lower and higher retention from the ICOone device respectively. Regarding deposition in the nasal cavity, all DSM batches display a similar pattern when used with the ICOone Nasal device. The powder primarily adheres to the nasal vestibule and atrium area, with no powder reaching the olfactory region. Notably, DSM-A exhibits an even distribution without agglomerates, whereas DSM-S shows the presence of agglomerates.

Populärvetenskaplig sammanfattning

Nasal administrering är en administeringsmetod där läkemedel inhaleras genom näsan. Metodens huvudsakliga syfte är att snabbt och effektivt behandla lokala symtom. Men på senare tid har det även ökats intresse för att uppnå en systemisk effect, där läkemedlet når blodomloppet och därigenom påverkar hela kroppen.

Näshålan är ungefär 15-20 ml, med en yta på cirka 150 cm^2 och är uppdelad i två symmetriska icke-sammanlänkade halvor. Varje halva är indelad i olika regioner med specifika funktioner. Den främre delen, vid näsborren, kallas nasal vestibul och är täckt av hud och hår. Läkemedel som når detta område filtreras bort. De återstående områdena är täckta av nässlemhinnan. I atrium är det svårt för läkemedel att sprida sig till blodomloppet, medan den respiratoriska regionen, även känd som andningsrelaterade regionen, spelar en viktig roll för att administrera läkemedel. Rik blodförsörjning i detta område underlättar absorptionen av vissa läkemedel och molekyler till blodomloppet. Det innebär att läkemedel som tas upp genom näsan, särskilt mindre stabila proteiner, har högre absorption jämfört med när de tas oralt. I den del av näsan som kallas för olfaktoriska regionen, vilket är området i näsan där luktsinnet finns, kan vissa läkemedel passera blod-hjärnbarriären (BBB), vilket möjliggör direkt leverans till centrala nervsystemet.

Majoriteten av dagens läkemedel som administreras via näsan är flytande trots nackdelarna med denna formulering. Näsmediciner i flytande form kan snabbt elimineras från näshålan, vilket minskar kontakttiden med målorganet och därmed reducerar deras effektivitet. Näspulverformuleringar erbjuder fördelar jämfört med vätskor, inklusive bättre motståndskraft mot mucociliär rening (självrensande mekanism), enklare sammansättning, högre dosering möjligheter och förbättrad stabilitet. Pulverformuleringar möjliggör användning av speciella hjälpmedel, såsom mucoadehsiva polymerer, som kan öka uppehållstiden i näsan.

I detta arbete har fyra nedbrytbara stärkelse mikrosfärer (DSM) med mucoadhesiva egenskaper, kallade DSM-A, DSM-S, DSM-T och DSM-L, utvärderats som hjälpmedel för nasal läkemedelsadministration. Deras fysiska och kemiska egenskaper har studerats och även deras prestanda som pulver har testats i kombination med den nasala enheten, ICOone Nasal. Dessutom studerades deras deponeringsprofiler genom att använda en 3D-printad modell av näshålan.

Enligt resultaten visade studien att DSM-A uppvisade de mest önskade egenskaperna för nasala läkemedelspulver och fungerade bra i kombination med nasal enheten ICOone. Detta gör DSM-A till det mest fördelaktiga pulvret som bärare för nasal läkemedelsadministrering. DSM-S hade oönskade egenskaper och visade dålig kompatibilitet med ICOone Nasal-enheten vilket gör DSM-S till den minst föredragna som bärare för nasal läkemedelsadministrering.

Contents

1 Background

Intranasal drug delivery is an administration method in which drugs are insufflated through the nose. The predominant factor for this route of administration is to offer a practical and accessible method for quickly and effectively treating localized symptoms. However, the interest in the delivery of drugs to systemic circulation is increasing. Drug molecules, both small molecules and biomacromolecules, can quickly be absorbed into systemic blood circulation through the nasal mucosa avoiding first-pass metabolism. Drugs like protein and peptides delivered via nasal systems exhibit greater absorption than oral administration. This might be caused by the tissue's high permeability, vascularization, and restricted enzymatic activity. The blood-brain barrier (BBB) typically prevents drugs from traveling from the bloodstream to the brain, but if drugs can travel along the olfactory neurons at the top of the nasal cavity, they can bypass the BBB and go directly to the brain. [1]

Today, the majority of nasal pharmaceutical products on the market are liquids despite the many drawbacks of this formulation. The microbiological and chemical instability of nasal liquids, the relatively high formulation volume supplied to ensure medicine dosing, and the rapid clearance from the nasal cavity are all significant drawbacks. Nasal powder presents a chance to enhance pharmacological effects by, among other things, enhancing mucosal clearance, which increases the time the drug is in contact with the target. This is because special excipients can be used in powders, of which mucoadhesive polymers appear to have the greatest potential to increase the residence time in the nose.[2] To ensure the required shelf life, liquid compositions need stabilizers, additives, and correct storage conditions. Powder formulations could have a simpler composition and allow for larger administration doses. They also have the advantage of enhancing drug diffusion and absorption across the mucosa compared to liquid forms, which have been shown to have low and variable drug bioavailability.[3]

1.1 Purpose of the work

This project aims to investigate the potential use of degradable starch microspheres (DSM) as a carrier for nasal drug administration. Four different DSM batches, namely DSM-A, DSM-S, DSM-T, and DSM-L, will be evaluated to determine their physicochemical characteristics. Furthermore, powder performance testing will be conducted to assess the flow properties of the powder, ensuring consistent dosing and smooth flow through the delivery device, ICOone Nasal. A 3D-printed nasal cavity model will also be used to determine their respective deposition profile. During the evaluation, the DSM batches will be compared with Nasaleze, a nasal powder available on the market. The findings from this study will provide valuable insights for developing effective nasal drug delivery systems.

The following research questions will be explored:

- How does moisture affect the different DSM qualities?

- How are the different DSM qualities distributed and deposited within the nasal cavity?
- Is there a risk of DSM inhalation into the lungs?
- How does DSM function in the Iconovo nasal device (ICOone Nasal)?

2 Theory

The following theory section will overview the nasal cavity and its different segments. It will also discuss the importance of efficient drug delivery to the targeted site in the nasal cavity and the challenges associated with achieving this. The section will then introduce degradable starch polymers as a potential solution for improving nasal drug delivery.

2.1 Nasal cavity

The nasal cavity is an air-filled body part, roughly 15-20 mL, with a surface area of about 150 cm^2. The role of the cavity is to make breathing possible as well as olfaction and environmental protection. Therefore, the cavity's structural and histological features support these functions. [4] The cavity is separated into two non-connected symmetrical parts, the left and right nasal cavities, by the nasal septum dividing the two nostrils. Each part of the cavity is lined with two different tissues called the nasal vestibule, the skin-lined portion, and the nasal cavity proper, the mucosa-lined portion. The mucosa-lined portion is divided into three regions called the atrium, the respiratory region, and the olfactory region, displayed in Figure 1.1. [4][5]

The nasal valve separates the nasal vestibule from the nasal cavity proper. It acts as a transitional zone between these two areas and regulates airflow during breathing. [6] The nasal vestibule is inside the nostril and covers about 0.6 cm^2. The anterior of the nasal vestibule is covered with hair, called vibrissae, whose function is to filter the incoming air from dust and other material. The area has a low permeability with poor vascularization making the absorption of substances such as drugs very difficult. [4]

The nasal cavity proper does not have any hair but instead is lined by mucosa, a moist tissue containing lots of secretions. [5] The atrium has low vascularity and reduced permeability. However, the respiratory area has very high vascularization and good permeability.[4] Hence, the region plays a significant role in nasal drug delivery due to the rich blood supply in this region facilitating the absorption of certain drugs and molecules from nasal formulations into the bloodstream. [7] The respiratory area covers the largest part of the nasal cavity, having a high surface area of 130 cm^2. The olfactory segment is located in the uppermost part of the nasal cavity, having a surface area of approximately 15 cm^2. [4] The primary function is detecting and processing odor molecules to capture and transmit sensory information related to smell to the brain. The unique anatomical connection of the olfactory segment to the brain enables bypassing the blood-brain barrier (BBB), allowing direct delivery of certain medications and therapeutic agents to the central nervous system. [4] The area is, therefore of interest in nasal drug delivery because certain medications and therapeutic agents can be targeted to this region for the treatment of olfactory-related disorders or neurological conditions. [7]

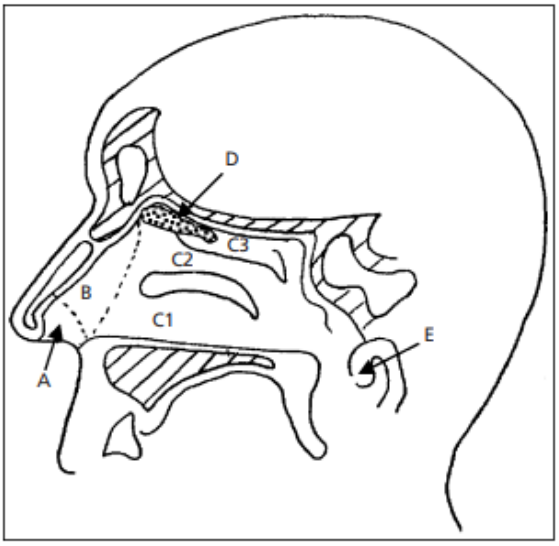

Figure 1.1. The sagittal cross-section of the nasal cavity displays the nasal vestibule (A), atrium (B), respiratory area: inferior turbinate (C1), middle turbinate (C2) and superior turbinate (C3), the olfactory region (D), and nasopharynx (E). [8]

2.1.1 Nasal mucosa

The nasal mucosa is a specialized tissue that lines the nasal cavity and plays a crucial role in respiratory and olfactory functions. Different layers of the nasal mucosa work together to fulfill various functions. Olfactory and respiratory epitheliums compose the outermost layer, which differ in function. Respiratory epithelium is thinner than olfactory epithelium. [9] Both epithelium types have numerous cilia, but the olfactory epithelium has modified cilia that function as olfactory receptors to detect and transmit odor signals. [10]

The underlying tissue supporting the nasal mucosa is the lamina propria and contains blood vessels, nerves, and various glands. The Epithelial cells are anchored to the underlying tissue by a basement membrane, an extracellular matrix providing structural support. [4]

2.1.1.1 Mucociliary clearance

Mucociliary clearance is a vital innate defense mechanism responsible for removing unwanted particles inhaled and deposited within the nasal cavity and subsequently trapped by the mucus layer. The airway surface liquid comprises the periciliary layer and the mucus layer, covering the ciliated epithelial cells that line the nasal mucosa. The mucus, present atop the cilia, acts as a protective gel-like barrier and is composed of water, carbohydrates, proteins, and lipids, giving it adhesive and viscoelastic properties. The mucus layer entraps the unwanted foreign particles and pathogens, preventing them from reaching the deeper parts of the respiratory system. [11]
The periciliary layer has a low viscosity and covers up to the cilia's height. The coordinated interaction of these layers facilitates the movement of the cilia that beat rapidly in a coordinated fashion, creating a wave-like motion that propels the mucus layer along the nasal cavity. [11]

For nasal drugs in liquid or powder formulations lacking mucoadhesive properties, the half-life of mucociliary clearance is typically around 15-20 minutes. This indicates that the nasal cavity efficiently clears substances not strongly adhering to the mucus layer. [12]

2.2 Nasal Drug Delivery

The physical characteristics and the powder performance of nasal powders play a crucial role in achieving the desired therapeutic effect. It can affect the deposition pattern and bioavailability of the drug, and therefore, careful consideration must be given when selecting and optimizing these properties. For instance, when targeting nose-to-brain delivery, the powder must be designed to reach the olfactory region specifically. [13]

One of the issues related to nasal drug delivery is the mucociliary clearance mechanism. Mucoadhesion is a mechanism that can be employed to improve the residence time of the drug at the site of action. Microparticles made of polymers can encapsulate the API and enable controlled drug release over a prolonged time. Mucoadhesion is a crucial factor in achieving this sustained release. [14]

2.2.1 Powder physical characteristics

Particle characteristics are critical for nasal drug delivery, as it affects drug performance. Particles smaller than 10 μm can improve drug dissolution in the nasal mucosa. However, there is a chance of lung inhalation during delivery. [15] To achieve optimal deposition within the nasal cavities, it is recommended to use particles with a median size ranging between 30 and 120 microns. Particles larger than the recommended size range are prone to depositing near the front of the nose or being prevented from entering the distal portions of the nasal cavity. This limitation occurs as they become trapped in the nasal valve region or on the front surface of the turbinates. [16] Thus, the particle size is one factor affecting the deposition profile of the powder. For example, particles with an aerodynamic diameter of 20 micrometers or less are preferred for nasal drug delivery to the olfactory region. [13]

The capacity of the nasal cavity for dry powder drug administration varies depending on individual factors and the specific dry powder formulation used. Higher quantities can potentially irritate the nasal mucosa. Minimizing the use of non-active substances is crucial for delivering high API doses to the nose. [2] Additionally, combining a larger surface area with smaller particle sizes maximizes drug delivery efficiency. Scrunchy particles, characterized by their high specific surface area, offer advantages in nasal drug delivery. Their larger surface area leads to more efficient deposition in the nasal cavity and enhanced drug delivery per dose. Scrunchy particles also demonstrate improved dose uniformity and less variation than particles with smoother surfaces. Reduced interparticle interactions among scrunchy particles minimize aggregation, enhancing the dispersibility and stability of the nasal drug formulation. This results in better aerosol performance and efficient drug delivery to the target regions of the nasal cavity. [17]

2.2.2 Flowability

In dry powder nasal administration, flowability refers to the ability of powders to flow freely and uniformly. Understanding the concept of flowability is essential as it influences the handling, packaging, and dispersion of powders within the nasal cavity. [18]

The Ph. Eur. definition of nasal powders requires the formulation to be combined with a device for nasal insufflation. The deposition of particles depends on the interaction between the formulation and delivery system. [19] Depending on which device is being used, a different deposition profile may be generated due to them using different mechanisms. For example, nasal powder sprays, Breath-actuated powder inhalers, and nasal powder insufflators exhibit different mechanisms resulting in different deposition patterns and effectiveness of drug delivery in the nasal cavity. Powder sprays use a compressible compartment to generate a plume of particles when pressed and released. Nasal powder insufflators require the patient to blow into a mouthpiece, creating airflow that propels the powder into the nose. Breath-actuated powder inhalers rely on the patient's breath to empty a blister or capsule, delivering the powder as they inhale. [19][20] The inspiration rate can also vary amongst patients, with an average resting flow rate of 20-30 liters per minute (LPM), which can increase during exertion or acute distress to exceed 45 liters per minute. [21]

Nasal powders require good flowability for proper dispersion and fluidization upon actuation, as well as for filling into a capsule or device. [2] A poorly flowing powder can result in uneven deposition and agglomeration, impeding delivery to the desired target area. Particle cohesion is the primary factor affecting powder flowability, caused by electrostatic and van der Waals forces. Cohesive forces can cause agglomeration, leading to non-uniform dispersion and deposition in the anterior nasal parts, preventing delivery to the desired target area. Therefore, minimizing cohesive forces between particles is crucial to prevent agglomeration. [2][22]

2.2.3 Mechanism of mucoadhesion

Microparticles made of polymers with mucoadhesive characteristics play a crucial role in nasal drug delivery by increasing the contact time between the drug and the nasal mucosa. [23] Such polymers are gelatin, starch, chitosan, and cellulose derivatives, commonly used in nasal drug formulations. [23][24] The interaction between polymers and biological tissues in mucoadhesion is facilitated through hydration, leading to the liberation and interaction of polymer chains. When dry particles containing polymers come in contact with nasal secretions, a process occurs where the polymer chains hydrate while the secretions undergo dehydration. [19] This results in increased residence time due to the increased mucus viscosity caused. The increased resistance arises from a reduction in the frequency and/or amplitude of ciliary beats, thereby impairing the effectiveness of the mucociliary clearance system. The surrounding fluid or mucus physical properties directly influence cilia's movement. [23][19]

Additionally, during hydration, the hydrogen bonds within the polymer chains dissociate, enabling their interaction with the mucosal polymer chains. The chains intermingle and entangle to form semi-permeable adhesive bonds, which impede ciliary movement, resulting in extended retention time in the nasal cavity, see Figure 1.2. [25] Optimal mucoadhesion requires a critical degree of hydration, as incomplete hydration limits the liberation of polymer chains. In contrast, excessive hydration weakens the mucoadhesive bond. [23]

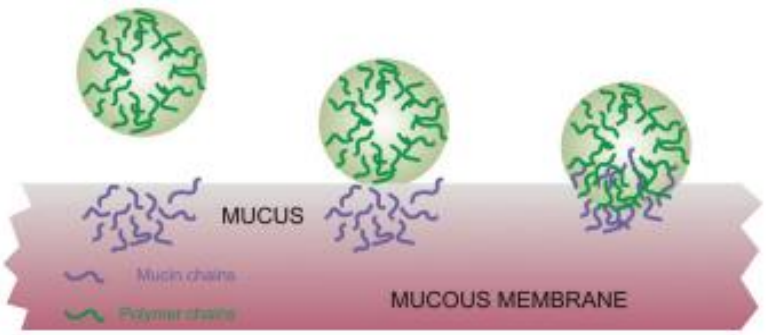

Figure 1.2. Interaction between bioadhesive and mucosal polymer chains. [26]

2.2.3.1 Degradable starch polymers

Degradable starch microspheres (DSM) are polymers that are bioadhesive, biodegradable, and biocompatible. As the DSM comes in contact with the aqueous mucosa, it starts to swell forming a gel-like system. As described earlier, this process enhances the duration of contact between the mucosa and the drug. [27]

Our body contains alpha-amylase that breaks down the degradable starch particles into smaller molecules that the body can easily absorb. Once the particles are broken down, the resulting degradation product, glucose, can be metabolized by the body's natural processes and eliminated through normal bodily functions. Sphere degradation rates are influenced by the size, internal cross-linking, added compounds, and source material, affecting drug release and treatment duration. Producers can develop customized drug delivery systems by knowing the degradation rate to meet desired requirements. [28] Furthermore, microsphere formulation using permeation enhancers has been shown enhanced drug release rates and increased surface area. Additionally, the microspheres have shown effective absorption of protein-based drugs, such as human insulin and human growth hormone, making them promising in drug delivery applications. [29]

One of the advantages of these microspheres is their degradability, meaning that they can be broken down in the body over time, releasing the drug gradually and reducing the potential for toxic effects associated with the rapid release of non-dissolved residues. [28]
Also, the starch microspheres do not trigger an immunological reaction reducing the risk of adverse immune reactions or hypersensitivity reactions that can occur with some other types of drug delivery systems. Therefore, the drug can be delivered to patients with allergies or other immune disorders without causing additional complications. [27]

1.3 Analytical methodologies

1.3.1 Scanning electron microscope

A scanning electron microscope (SEM) is used to examine the fine structure and morphology of a wide range of materials at high magnifications. It works by producing a beam of high-energy electrons that interact with the analyzed sample, generating secondary electrons, backscattered electrons, and other signals that are detected by the instrument and processed to form an image. [30] Detailed information about the material's surface, including topography and texture, can be generated by controlling the conditions under which the beam interacts with the sample. This could for example be the angle and energy of the electrons. Even though the SEM instrument is mainly used for high-magnification images, low-magnification images could also be generated, which provide a broader view of the sample's surface. [31]

1.3.2 Particle size distribution by laser diffraction

Particle size distribution (PSD) analysis is a widely employed technique for characterizing the size distribution of particles in a sample. Various instruments and techniques can be used to measure particle sizes, and laser diffraction technology is one commonly used approach in PSD analysis. The particle size distribution is determined by analyzing the scattering pattern produced when the laser beam interacts with the particles. This technique enables measurements of a broad range of sample types and sizes, in the range of 0.1 to 3000 microns. [32]

The analysis can be performed using either the dry method or the wet method, depending on the nature of the sample. In the dry method, the particles are dispersed by dry air, and in the wet method, the sample is dispersed in a liquid medium before analysis. Even though both methods have their own advantages, using both can sometimes provide additional information. [32]

1.3.3 Gravimetric vapor sorption

Gravimetric vapor sorption (GVS) is an analytical technique used to measure the amount of moisture or other volatile compounds absorbed and desorbed by a solid material as a function of the relative humidity (RH). The principle of the method is based on the fact that most materials can absorb moisture from their surroundings, which can affect their physical and chemical properties. In a typical isotherm measurement, the sample is exposed to a controlled environment of varying pressure, thus RH, at a constant temperature. By measuring the resulting changes in weight, it is possible to determine the moisture sorption isotherm of the material. The isotherm provides information about the material's moisture uptake and release characteristics and may give additional information, e.g., of the presence of micropores. [33]

1.3.4 Specific Surface Area (SSA)

BET-specific surface area (SSA) testing is a measurement technique used to determine the surface area of a solid material, such as a powder or porous material. "BET" stands for Brunauer, Emmett, and Teller, who developed the calculation method. [34]
The BET method involves adsorbing a gas, typically nitrogen, onto the material's surface at varying pressures and measuring the amount of gas adsorbed at each pressure. The gas pressure, temperature, the kind of gas used as well as the surface area of the material determines how much gas that can be absorbed. The specific surface area of a material can be calculated by plotting the amount of gas adsorbed versus the pressure. The BET method is considered reliable and accurate for determining surface area, considering the material's external and internal surface areas. [35]

1.3.5 Pycnometer

The pycnometer is widely used to determine the volume of solid materials, including powders. It operates based on the principle of gas displacement, where gas is introduced into a chamber containing the powder and Boyle's Law of gas expansion is utilized to accurately calculate the true density of solid materials. In the pycnometer method, the powder sample is accurately weighed and placed in a container with a known volume, typically a small chamber or cell. The container is then filled with a gas, such as helium (He), which displaces the air and fills the voids within the powder bed. The increase in pressure resulting from the gas displacement is measured, allowing the calculation of the powder volume. The true density of the material is obtained by dividing the obtained volume by the sample weight. [36]

1.3.6 SprayTec

The SprayTec method, based on laser diffraction technology, is a powerful analytical technique commonly used for studying inhalation aerosols, including nasal powders. It operates on the principle of measuring the scattering of laser light by particles in a spray or aerosol (see section 1.3.2). The method provides real-time measurements, allowing investigation of the dynamics of particle size distribution during spray or aerosol generation. Moreover, it directly measures the particle size distribution from the corresponding delivery devices, providing valuable insights into the performance and efficiency. [37]

2 Experimental

This chapter aims to elucidate the experimental procedures conducted in this study. The materials and equipment employed will be presented for each experiment, along with an explanation of their respective applications and procedures.

The experimental analyses aimed to evaluate the physical and chemical properties of the microspheres, as well as the powder performance, using various techniques, including scanning electron microscopy (SEM), particle size distribution (PSD) analysis, bulk density measurements, gravimetric vapor sorption (GVS) studies, pycnometer measurements, BET analysis, powder flow (Angle of Repose) determination, SprayTec analysis, and nasal cast analysis.

The PSD analysis, angle of repose determination, SprayTec analysis, and nasal cast analysis were specifically conducted on the DSM batches subjected to different storage conditions. These experiments aimed to provide insights into the microspheres' behavior and performance under various storage conditions.

A commercially available over-the-counter nasal spray called Nasaleze, which consists of microcrystalline cellulose. This study used it as a reference to compare its properties with the DSM batches. Nasaleze was sourced from Nasaleze International Ltd and obtained in its original package, a nasal spray pump. The reference drug was handled and stored according to the recommended storage conditions specified by the manufacturer. PSD, SEM, Angle of repose determination, SprayTec, and nasal cast analysis were also applied to Nasaleze to compare and evaluate their properties accurately.

2.1 Scanning electron microscope

The SEM analysis was conducted using the equipment in Table 2.1.

Table 2.1. The equipments used in the SEM analysis and its corresponding models.

Equipment	Type
Sputter coater	Cressington 208 HR
Scanning Electron Microscope	Tescan Mira 3

The DSM microspheres and Naasaleze were dispersed onto adhesive carbon tape placed on an SEM sample holder stub. An 18 nm, 40 mA Pt/Pd film was applied as a coating to enable conductivity. The material was analyzed using scanning electron microscopy (SEM) at various magnification levels. This allowed for a comprehensive assessment of both the overall particle and agglomerate morphology and a close examination of the surface structure

of individual particles. The analysis was initialized using the following settings presented in Table 2.2.

Table 2.2. The various parameters and their respective settings employed in the SEM analysis.

Parameter	Setting
Imaging mode	Secondary Electron Imaging
Sample condition	4 kV, WD = 4-5 mm, 50-1000x

WD=working distance

2.2 Particle size distribution

The PSD analysis was divided into two parts, denoted as Part I and II. In Part I, the PSD analysis was carried out on all four batches of DSM as well as Nasaleze, using a suspension-based approach. The samples were stored in a dry condition in a desiccator cabinet, maintaining a RH level of less than 5%, prior to analyses.

In Part II, PSD of dry powder analysis was conducted on only DSM-A and DSM-S. These batches were stored in the desiccator cabinet under dry conditions with an RH level of less than 5%. Additionally, each batch was added to three glass vials of 10 ml and subjected to varying RH levels (53%, 75%, and 94%) for five days.

2.2.1 Part I - Powder in suspension

The instrument used was a Malvern Mastersizer 3000 instrument, equipped with a 300 mm reverse Fourier lens and Hydro MV sample cell and stirrer. The Hydro MV sample cell was filled with isopropanol which was used as the dispersion medium. Approximately one spoon of the sample was added to the cell containing isopropanol. The setting parameters were selected, as seen in Table 2.3, and the measurement was initiated.

Table 2.3. The parameters utilized in the PSD analysis in suspension and their corresponding values.

Parameter	Value
Background measurement time	10 s
Obscuration	15-35%
Sample measurement time	10 s
Number of measurements	3
Delay between measurements	0 s
Dispersant refractive index	1.39

Analysis model	General purpose
Particle refractive index	N/A (Fraunhofer)
Absorption index	N/A (Fraunhofer)
Stirrer speed:	2500 rpm
Sonication	60 s duration at 20% and 180 s at 60%

2.2.2 Part II - Dry powder

For this experiment, Malvern Mastersizer 3000 instrument, equipped with a 300mm reverse Fourier lens and Aero S sample cell was used. Approximately two spoons of the sample were added directly to the Aero S feeder funnel. The measurements were done using the following settings displayed in Table 2.4.

Table 2.4. The parameters utilized in the PSD analysis in dry and their corresponding values.

Parameter	Value
Background measurement time	10 s
Sample measurement time	15 s
Number of measurements	1
Obscuration lower limit (%)	0.1
Obscuration higher limit (%)	50
Dispersant refractive index	1.00
Air pressure	0.3-3 bar
Analysis model	General purpose
Particle refractive index	N/A (Fraunhofer)
Absorption	N/A (Fraunhofer)

2.3 Bulk density

To determine the bulk density of the samples, a cylinder with a known volume of 5.2 cm^3 was employed. The cylinder was placed on a scale, and the scale was tared to zero. The sample was then carefully added to the cylinder until it overflowed, ensuring that no compression or

compaction of the powder occurred. Any excess powder at the top was gently removed by scraping. Next, the cylinder filled with the sample was placed back on the scale, and the weight was measured. This process was repeated three times, and the average mass value was calculated. The bulk density was then calculated using the following equation:

$$Bulk\ density\ =\ m_{sample}\ /\ V_{cylinder} \quad (1)$$

The method described above was conducted for all DSM batches to calculate the bulk density.

2.4 Gravimetric vapor sorption

Approximately 10 mg of the sample was carefully placed into an aluminum (Al) pan and positioned inside the experimental instrument. The sample was subjected to a series of stepwise RH changes during a single cycle, following the sequence: 20-30-40-50-60-70-80-60-40-20-0% RH. These RH changes were executed using the open-loop mode of the SMS DVS Advantage instrument.

The experiments were conducted at a constant temperature of 25 °C, with a gas flow rate of 200 ml/min gas flow rate. During the RH cycling, the criterion for the rate of change in mass (dm/dt) was set at 0.001 weight-%/min within a 5-minute window. The maximum allowed time for each step, except for the 0% RH steps, was set to 150 minutes. The 0% RH steps did not have a specific dm/dt criterion but were set to run for 6 hours.

The same method described above was conducted for all DSM batches to evaluate their respective moisture interactions.

2.5 BET

The TriStar II Plus 3030 instrument from Micromeritics was utilized for the experiment. Four glass tubes were weighed and each filled with the DSM batches and subjected to a degassing process at room temperature for 18 hours. This process involved a continuous flow of nitrogen gas (N2) to eliminate loosely bound molecules on the external surface and from potential channels within the material. Following degassing, the glass tubes were weighed again and then placed into the measuring positions within the instrument.

The measuring positions were set at -196 °C, which corresponds to the boiling point of liquid nitrogen. The tubes were evacuated and exposed to a range of partial pressures, covering the Brunauer-Emmett-Teller (BET) region to assess specific surface area (SSA). Concurrently, the actual saturation pressure of the liquid nitrogen utilized in the experiment was continuously monitored. To ensure accurate measurement of nitrogen adsorption, the free volume within the tubes was determined by measuring helium gas (He) prior to the nitrogen adsorption step.

2.5 Pycnometer

The samples from the BET analysis were used in this experiment. The samples that were already degassed from the BET analysis were each transferred from the glass tube to a small beaker and put for 20 min in a desiccator cabinet, maintaining a RH level of less than 5%.

Before the measurement, the pycnometer was calibrated for a period of 30 minutes. The calibration process involved using a certified calibration kit, which determined all the necessary cell parameters using a metal sphere of accurately known volume. Following calibration, a metal container with a volume of 1 cm^3 was placed on a scale and the scale was then tared. The test cup was then filled with ¾ of the DSM sample and the weight of each sample was measured. The test cup containing the sample was transferred to the Accupyc 1330 micromeritics equipment and the measurement started. The true density was determined using the following settings displayed in Table 2.5. This process was repeated for all DSM batches.

Table 2.5. The different setting parameters utilized in the pycnometer experiment with the corresponding value.

Parameter	Value
Number of purges	10
Purge fill pressure	15 psig
Run fill pressure	15 psig
Number of runs	10
Equilibration rate	0.02 psig/min
Run precision	No

The true density for each DSM batch was calculated using the equation below.

$$True\ density\ =\ m_{sample}\ /\ V_{sample} \quad (2)$$

where m= weighted mass of the sample (g) and V = generated volume of the sample from the experiment (cm^3).

2.7 Powder Flow (Angle of Repose)

Before analysis, all DSM batches namely DSM-A, DSM-S, DSM-T, and DSM-L were stored in a desiccator cabinet, maintaining a RH level of less than 5%. Additionally, DSM-A and DSM-S were each added to two glass vials of 10 ml and subjected to RH levels of 53% and 75% for a duration of ten days.

The laboratory room was observed to have a RH value of 24%. To measure the angle of repose, a funnel-based equipment with accurate height readings (Prototypverkstaden) was employed. The drug substance was introduced into the funnel following the methodology outlined in the pharmacopeia (USP 1174 and EP 2.9.36). The substance was allowed to flow freely and accumulate on a circular area with a well-defined boundary until the height of the pile ceased to increase. By measuring the radius of the circular area and carefully recording the height of the substance pile, the angle of repose (AOR) was calculated from the following equation:

$$\text{AOR} = arctan(\frac{h}{r}) \quad (3)$$

where h=height of pile (mm), and r = radius of the circular area (mm).

All DSM batches was flowed from a height that corresponds to the setting 0 cm on the instrument except for DSM-S stored under 75% RH which flowed from the setting 1 cm on the instrument.

For DSM-S stored under dry conditions, the intended technique was not applicable where the powder flowed freely from a funnel. In this case, the powder had to be manually added using a spoon, carefully distributing it to the circular area with a height that corresponds to the setting of approximately -1 cm on the instrument.

2.8 SprayTec

Prior to conducting the SprayTec analysis, the ICOone Nasal devices, see Figure 2.1, were subjected to vacuum treatment for preparation.

Figure 2.1. The ICOone Nasal device.

Each device was assigned a sequential number for identification and weighed. For each DSM batch, six nasal devices were filled, ensuring that only 50% of the device's cavity was filled without compacting the powder. Among these, three devices from each batch were placed in a desiccator cabinet set at 53% RH, while the remaining three devices were placed in a cabinet set at 75% RH. Additionally, three devices from each DSM batch and Nasaleze were

filled in the same manner and stored at approximately 20 ± 5% RH, referred to as dry conditions. The devices were left for one day to reach equilibrium under the respective storage conditions and the following day, the filled devices were weighed. The RH in the laboratory room was observed to be approximately 20 ± 5% RH.

The experimental setup involved using the Malvern SprayTec instrument with the inhalation cell attachment with the matching ICOone nozzle set at an angle of 45 degrees, see Figure 2.2.

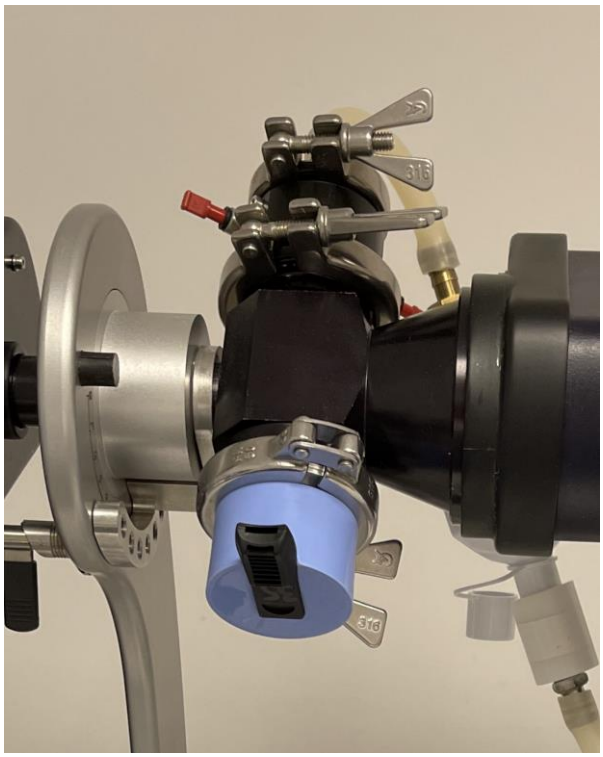

Figure 2.2. The setup for the SprayTec analysis with the ICOone nozzle and ICOone Nasal device attached.

The airflow was set to 30 L/min using a flow meter. The ICOone device was loaded into its corresponding nozzle, ensuring it is securely in place. The measurement was initiated and the suction time was set to 5 seconds. In total, the doses were analyzed for each batch stored under different conditions.

Furthermore, DSM-A and DSM-S were analyzed at flow rates of 20 and 40 L/min. Six nasal devices were filled with each batch, using the same manner. Three doses from each batch were analyzed at 20 L/min, and the other three doses were analyzed at 40 L/min, following the same process described above.

2.9 Nasal cast testing

Each device involved filling three ICOone devices. The same manner as when conducting SprayTec analysis was used where only 50% of the nasal device cavity was filled without being compacted. The device was weighed before and after being filled.

A 3D-printed nasal cavity model was used that replicated one of the two non-connected symmetrical parts, closely resembling the structure of the human nasal cavity. The nasal cavity is divided into two halves as seen in Figure 2.3.

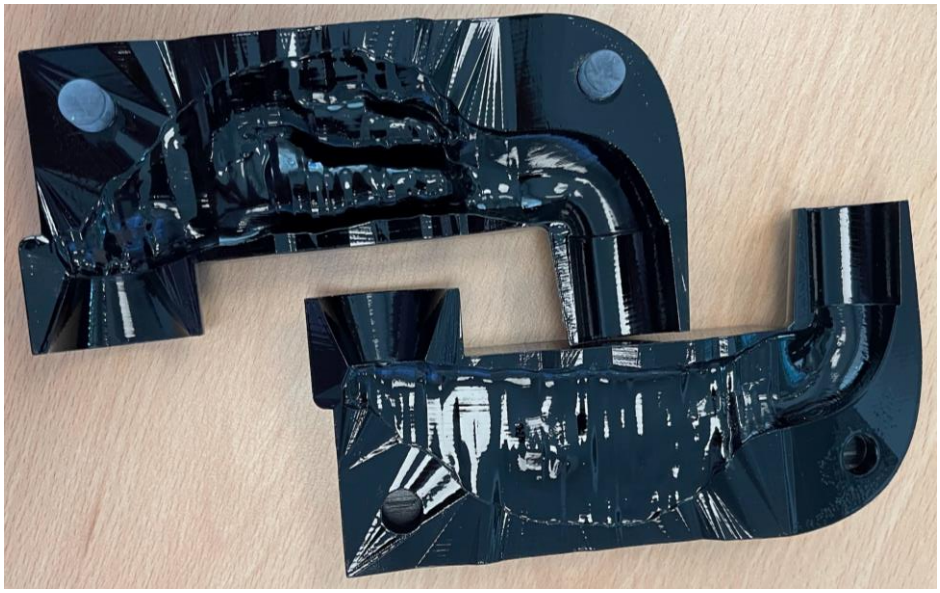

Figure 2.3. The 3D-printed nasal cavity model replicating the human nasal cavity. The two halvs together form one of the two nasal cavities.

Each half was coated with Bri glycerol and allowed to sit for 2 minutes. The two parts were then assembled and the nasal cast was fully wrapped using parafilm to ensure a complete seal and prevent any flow leakage. Additionally, the nozzle was added and was sealed entirely using adhesive pulp. The nasal cast was attached to a lab stand using a clamp. The setup was arranged to achieve an angle of approximately 45 degrees, following the configuration shown in Figure 2.4.

Figure 2.4. The setup of the nasal cast during nasal cast testing.

A filter was attached to the other end of the nasal cast that was further attached to a peristaltic pump using a hose. The flow was set to 30 L/min using a flow meter. The nasal device was

attached to the nozzle, ensuring it is securely in place and the measurement was initiated where the suction time was set to 5 seconds. Three doses were dispensed for each batch, and subsequently, the nasal cast was unwrapped to capture photographs.

The same preparation and analysis as described above were carried out at a flow rate of 40 L/min.

3 Results and discussion

3.1 SEM Images

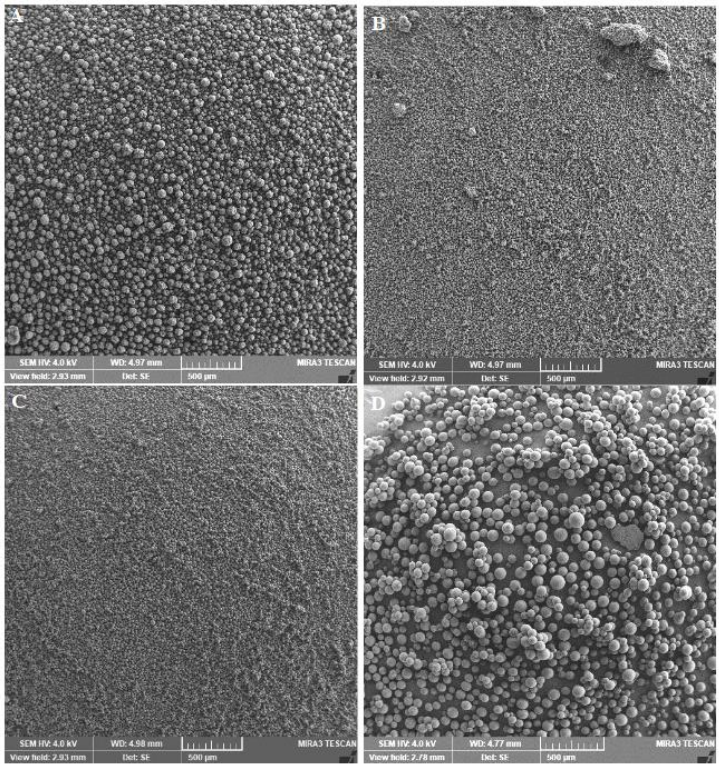

Figure 3.1 Low magnification SEM images of the four different batches. Image A represents DSM-A, image B represents DSM-S, C represents DSM-T and D represents DSM-L.

Figure 3.1 shows an SEM low-magnification image of four different DSM batches stored in a dry environment. Upon visual inspection, several notable differences can be observed between the batches. In images B and D, corresponding to DSM-S and DSM-L respectively, larger agglomerates of microspheres are visible. In contrast, DSM-A, shown in image A, and DSM-T (image C) have no visible agglomerates.

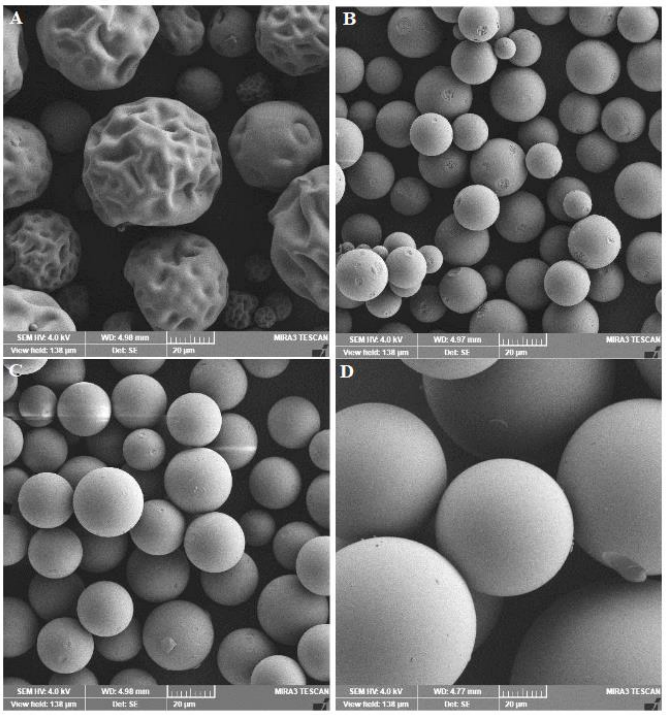

Figure 3.2 High magnification SEM image of the four different batches. Image A corresponds to DSM-A, image B to DSM-S, C to DSM-T, and D to DSM-L.

Figure 3.2 shows a high-magnification SEM image of four DSM batches with notable differences observed. DSM-A, shown in image A, has a unique "scrunchy" surface structure with irregular folds and creases. The remaining batches have smoother surfaces.

Overall, the observations made in Figures 3.1 and 3.2 indicate that there is a difference in the physical properties of the different DSM variants, particularly with regard to particle size distribution and the number of agglomerates present. DSM-A and DSM- T are the only batches having well-separated and evenly dispersed individual microspheres.

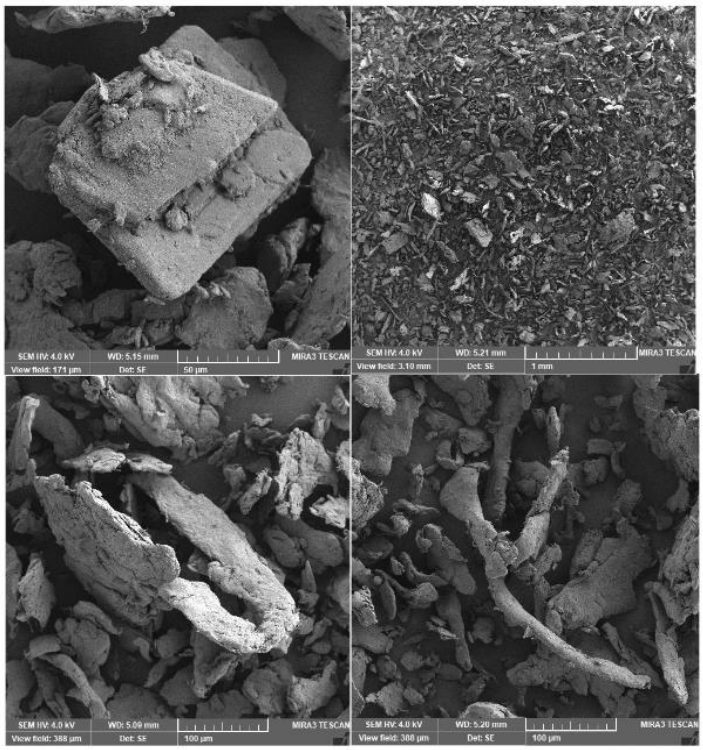

Figure 3.3 Four generated SEM images at different magnifications of Nasaleze.

In contrast to the DSM batches, the Nasaleze formulation does not contain spherical-shaped particles as shown in Figure 3.3. Examining images of the powder at various magnifications reveals that it lacks particles with a consistent, uniform structure. Instead, the powder is composed of particles that exhibit diverse appearances, with some having a branched structure and others having a more cubic structure.

3.1 PSD analysis of DSM batches

3.1.1 Analysis of powder in suspension

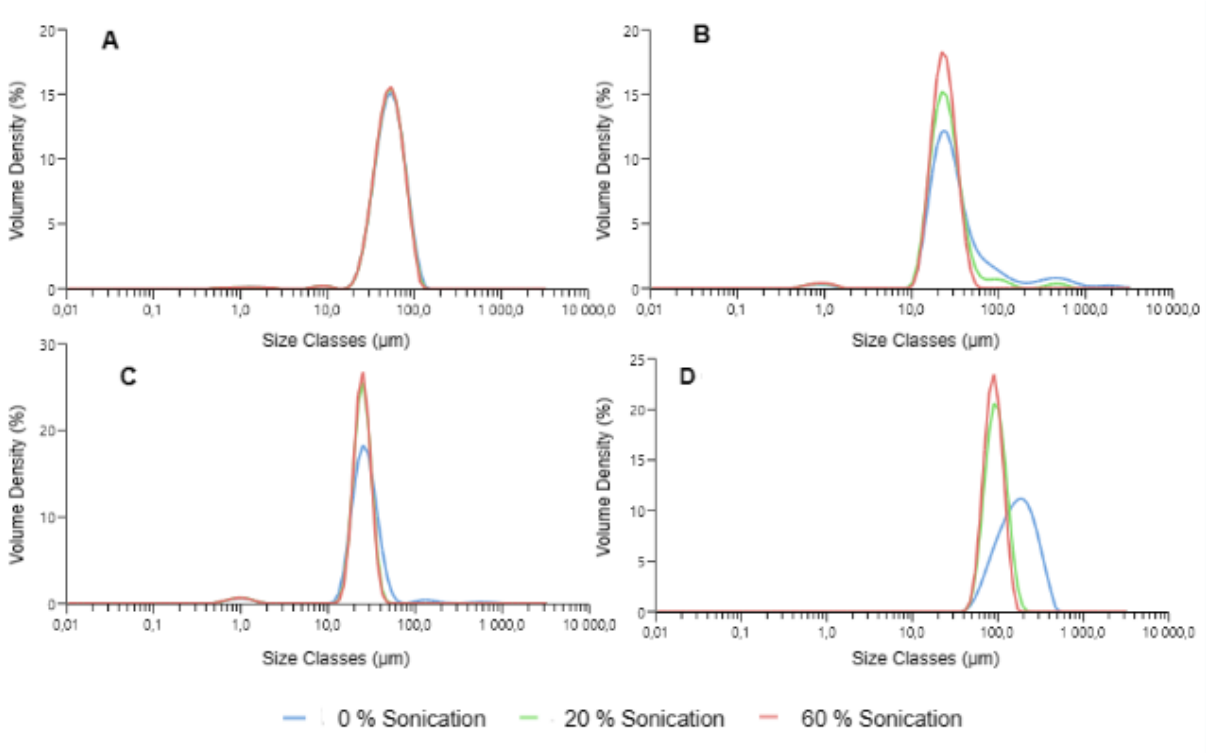

Figure 3.4 Generated four graphs from PSD analysis in suspension, with Image A corresponding to DSM-A, Image B to DSM-S, Image C to DSM-T, and Image D to DSM-L. The blue line in each graph represents the results from the experiment when magnifications were only stirred for 1 min, while the green and red lines, respectively, represent the results when 20% and 60% sonication power was added.

Figure 3.4 shows the graphs generated from analyzing the DSM grades at different sonication powers. The graphs representing DSM-A, seen in image A, have lines overlapping indicating that all particles are easily dispersible. However, the graph from DSM-S analysis, seen in image B, differs with the red line, corresponding to 60% sonication, having the smallest width and highest peak. In this case, a small peak with larger particles was observed after the main peak in the PSD graph, which disappeared as the sonication level increased to 60%. This is due to the agglomerates gradually disappearing with increasing sonication power. The analysis of DSM-T reveals a similar appearance as for DSM-S but to a less pronounced extent, seen in image C. The graphs get narrower and higher as the sonication level is increased. Also in this case, the small peak appearing after the main peak is disappearing with increasing sonication power. However, the peak is removed already at a sonication level of 20% compared to DSM-S where it was still remaining.

Lastly, for DSM-L seen in image D, as the sonication level is raised, the peak gets narrower and higher which is an indication of agglomerates being present. The agglomerates are removed at 20% sonication powder, as is the case for DSM-T. However, there is no curve

present before the main peak for this batch which could be due to this sample being sieved in advance.

Table 3.1. The PSD analysis in suspension at 60% sonication generated values for the parameters d50 and span for the different batches, DSM-A, DSM-S, DSM-T and DSM-L.

Sample	**d50 (µm)**	**Span**
DSM-A	51.9	0.99
DSM-S	23.5	0.85
DSM-T	24.9	0.59
DSM-L	90.1	0.65

The values of the parameters d50 and span presented in Table 3.1 indicate that DSM-L has the largest median particle size of 90.1 µm, with the second lowest span of 0.65 amongst all DSM batches. DSM-S and DSM-T have similar d50 values of 23.5 and 24.9 respectively. However, their span values differ with DSM-T having the lowest span value amongst all batches, indicating the narrowest particle size distribution. DSM-A has a d50 value of 51.9 µm and the highest span value of 0.99, indicating the highest particle size distribution.

The results from the PSD analysis in suspension indicate that DSM-A is the batch that has particles that are easily dispersible. The sample is not prone to agglomeration or clustering. However, for the other batches, sonication did affect the particle dispersion. For DSM-T and DSM-L, the agglomerates are removed already at 20% indicating that they can easily be removed. However, there are still some interparticle adhesion forces that in this case could easily be broken at a 20% sonication powder. For DSM-S, a higher sonication efficacy was required to remove the agglomerates indicating that there are stronger interparticle adhesion forces between the particles. Overall, the batches, except for DSM-A, were shown to have some tendency to form agglomerates with DSM-S having the highest cohesiveness and interparticle forces.

3.1.2 Analysis of dry powder

3.1.2.1 DSM-A

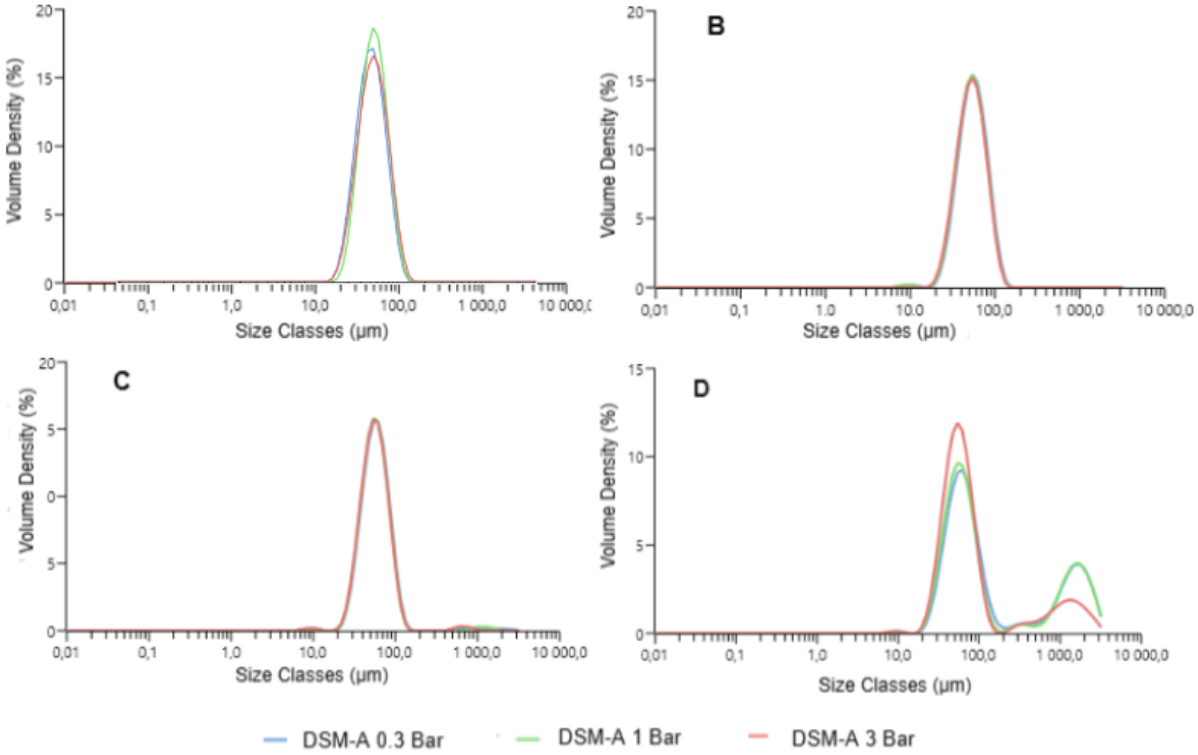

Figure 3.5. The figure displays the PSD analysis of DSM-A under different conditions. The blue, green, and red lines represent the analysis at 0.3 bar, 1 bar, and 3 bar, respectively. Graph A depicts the PSD analysis of DSM-A powder under dry conditions. Graphs B, C, and D demonstrate the PSD analysis of DSM-A powder at 53%, 75%, and 94% RH, respectively.

Figure 3.5 shows that DSM-A dry, DSM-A 53%, and DSM-A 75% are almost completely dispersed at the lowest pressure. However, for the powder stored at 94% RH, a peak after the main peak can be observed that decreases with increasing pressure. This indicates that at RH 94%, the powder forms agglomerates which are not seen for the other RH levels.

Table 3.2. The PSD analysis of dry powder at 3 bar generated values for the parameters d50 and span for the different DSM-A samples stored under dry, 53%, 75%, and 94% RH.

DSM-A at different RH	**d50 (µm)**	**Span**
Dry	55.1	0.97
RH 53%	53.5	1.00
RH 75%	56.9	0.99
RH 94%	62.2	17.44

The span values, in Table 3.2, for the powder stored at RH 0%, 53% and 75% is approximately equal. This indicated that the increase of RH from 0-75% did not affect the

span, however, it is significantly increased at an RH of 94%. These results suggest that powder stored at RH 94% gets a broader distribution. This can be attributed to the agglomeration of particles due to moisture absorption. At the high humidity condition of 94% RH, the particles become stickier, causing the particles to agglomerate. Moisture can change the surface chemistry of the particles, making them more adhesive or cohesive, and resulting in a broader particle size distribution.

The table above shows that the d50 parameter has a consistent value between 53.5-56.9 µm across the range of 0-75% RH. The highest value of 62.2 µm is observed at 94% RH. Despite these differences, there is no significant change in the value of d50 with changing RH values.

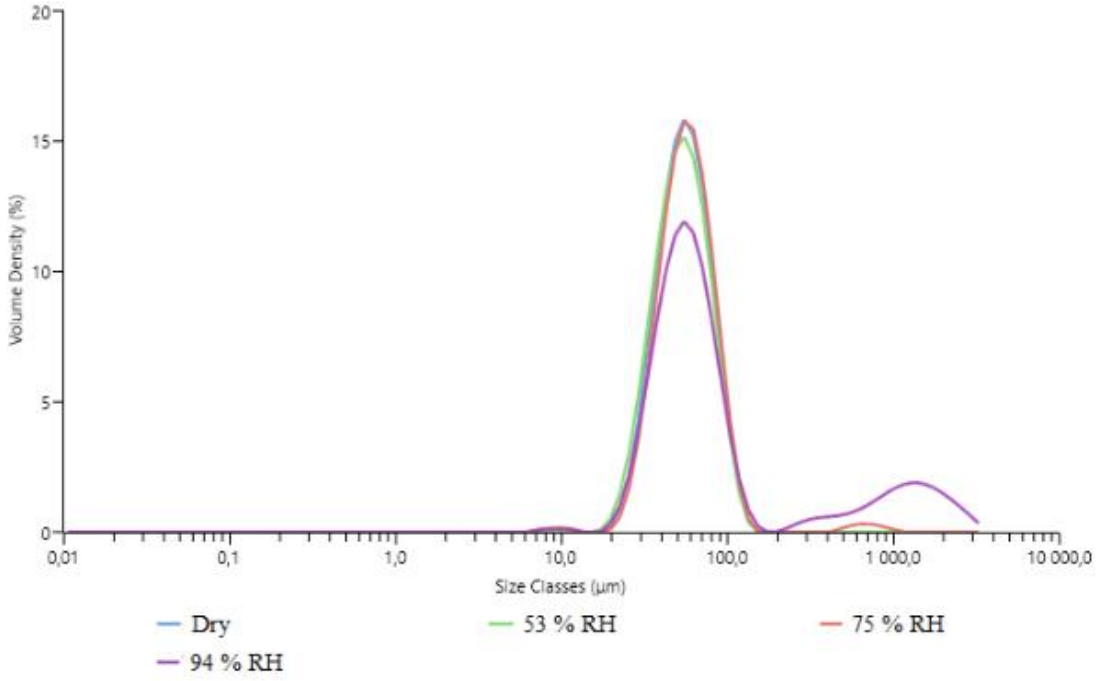

Figure 3.6. Graph generated from PSD analysis at 3 bar of DSM-A under different RH values. The blue line corresponds to the powder stored under dry conditions. The green, red, and purple line represents powder stored under 53%, 75%, and 94% RH respectively.

Figure 3.6 shows the comparison of the graphs generated from analyzing powder stored at different RH at 3 bar. The figure shows that none of the main peaks have moved to the right or left, indicating that the size of the spheres remains similar in value and thus does not seem to swell when stored at the tested range of RHs.

3.1.2.2 DSM-S

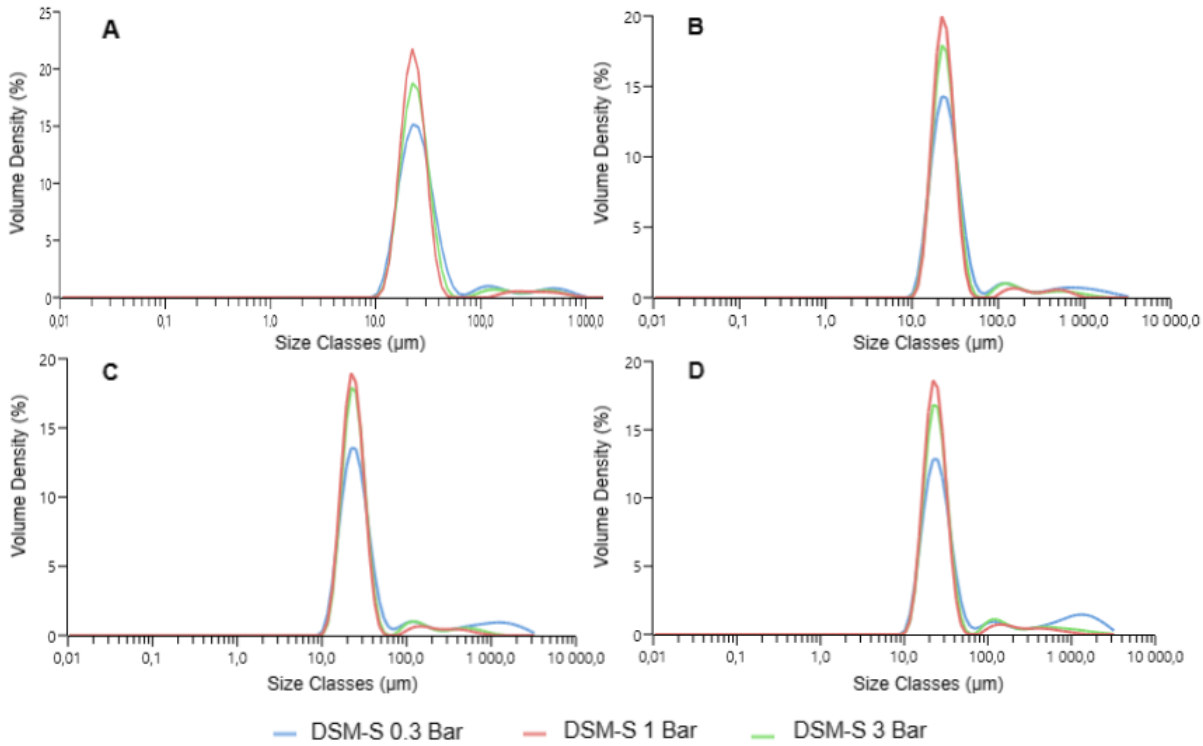

Figure 3.7. The generated graphs from the PSD analysis of DSM-S under various conditions. The blue, green, and red lines indicate the analysis conducted at 0.3 bar, 1 bar, and 3 bar, respectively. Graph A represents the PSD analysis of DSM-S powder under dry conditions. Graphs B, C, and D show the PSD analysis of DSM-S powder at 53%, 75%, and 94% RH, respectively.

Figure 3.7 shows that all powders stored under different RH conditions exhibited a similar pattern of increasing peak height with increasing pressure settings. The peak occurring after the main peak is decreasing with increasing pressure exhibiting a significantly higher peak at 0.3 Bar. However, in this case, the peak is present for all samples due to the fact that DSM-S, as opposed to DSM-A, contained agglomerates to begin with, before being exposed to elevated humidities.

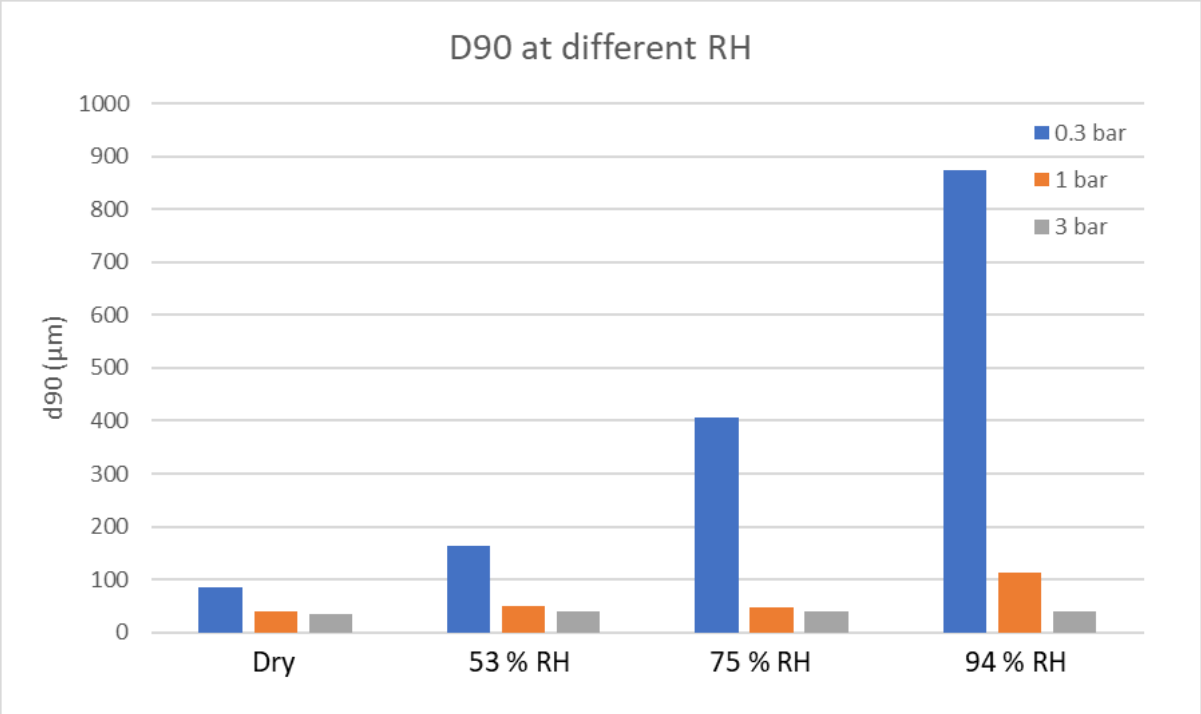

Figure 3.8. The generated d90 value from the PSD analysis of DSM-S stored under various conditions. The blue bar corresponds to the results from analyzing at 0.3 bar. The orange and gray colors correspond to results from analyzing at 1 and 3 Bar respectively.

The generated d90 value at different pressures, see Figure 3.8, shows that the value at 0.3 Bar for all conditions exhibits the highest value, with a noticeable difference from the other values. This is the reason for the notably lower main peak at 0.3 bar seen in Figure 3.7.

Table 3.3. The PSD analysis of dry powder at 3 Bar generated values for the parameters d50 and span for the different DSM-S samples stored under dry, 53%, 75%, and 94% RH.

DSM-S at different RH	d50 (µm)	Span
Dry	23.2	0.77
RH 53%	24.0	0.90
RH 75%	24.1	0.94
RH 94%	24.3	0.99

In Table 3.3 it can be observed that the d50 values do not vary significantly across the different RH values, ranging from 23.2-24.3 µm. However, agglomerates are being formed with increasing RH, seen as the increasing span value, and relatively higher d90 at 94% RH seen in Figure 3.8.

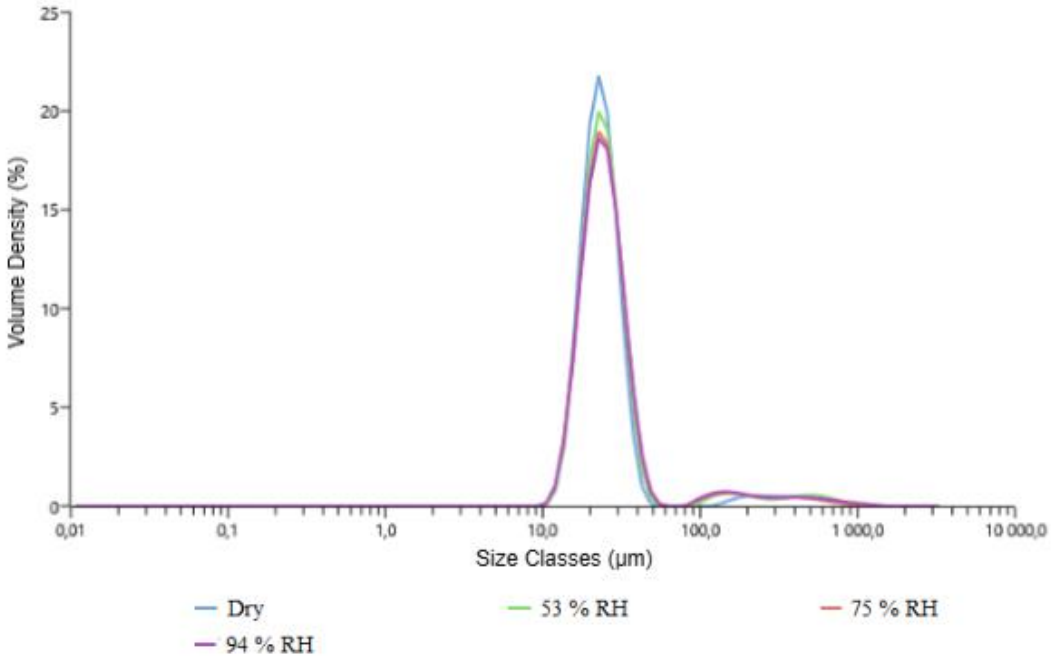

Figure 3.9. Graphs generated from PSD analysis at 3 bar of DSM-S under different RH values. The blue line corresponds to the powder stored under dry conditions. The green, red, and purple line represents powder stored under 53%, 75%, and 94% RH respectively.

Figure 3.9 shows the comparison of the graphs generated from all analyzed RH values at 3 bar. The results show that no peak has moved to the right nor left, as for DSM-A. This means that the average particle size and the distribution of particle sizes within the powder do not appear to change significantly with changes in RH, indicating no swelling, which can also be seen in Table 3.3.

3.1.3 PSD analysis of Nasaleze

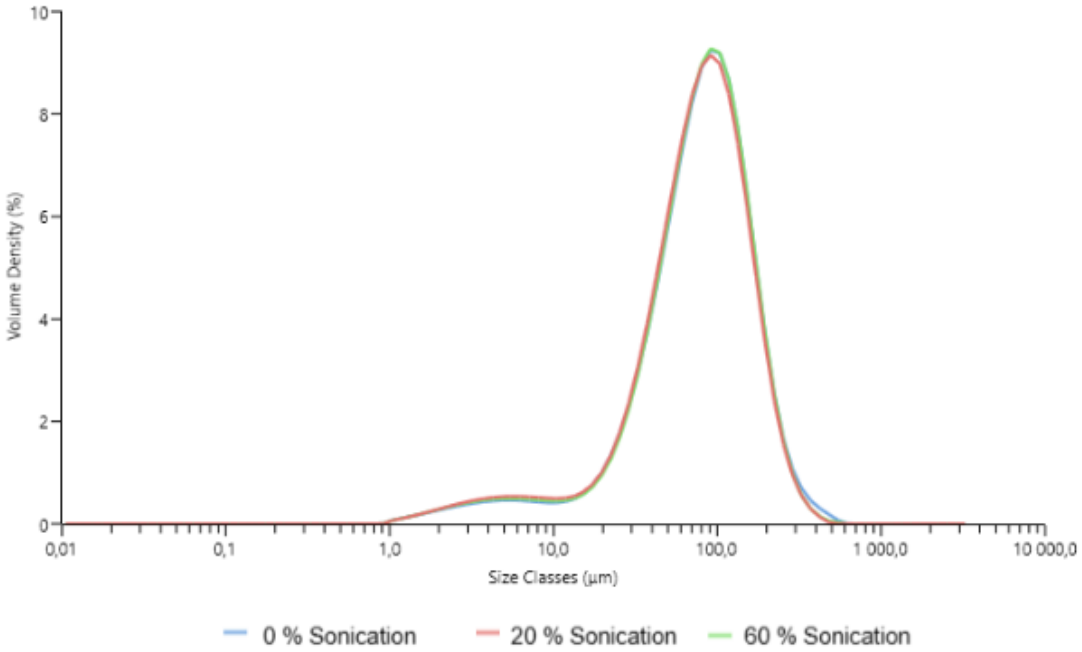

Figure 3.10. Generated graph from PSD analysis in suspension of Nasaleze, with Image. The blue line represents the results from the experiment when the solution was only stirred for 1 min, while the green and red line, respectively, represent the results when 20% and 60% sonication efficiency was added.

As seen in Figure 3.10, adding sonication did not affect the powder behavior of Nasaleze, seen as overlapping graphs. This was also observed for DSM-A indicating that both batches have particles that are easily dispersible.

Table 3.4. The values of the parameters d50 and span from PSD analysis of Nasaleze at 60% sonication.

Sample	**d50 (µm)**	**Span**
Nasaleze	79.8	1.87

The calculated span (1.87) for Nasalese is almost twice as big as the span value of DSM-A and the biggest amongst all batches, indicating a wider particle size distribution. This was expected since the particles exhibited diverse appearances and sizes, as seen in Figure 3.3. The mean particle size of Nasaleze, 79.8 µm, is almost as big as the mean particle size of DSM-L.

3.3 GVS

3.3.1 DSM-A

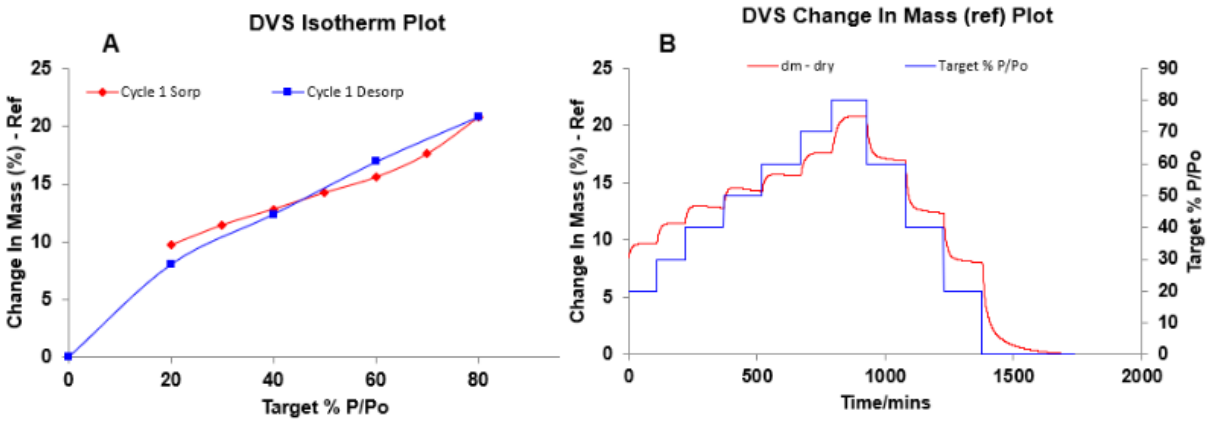

Figure 3.11. Image A display the correlation between the mass and relative humidity for DSM-A. The relative humidity is on the x-axis and the mass is on the y-axis. The blue line represents the desorption and the red line the absorption. Image B shows the change in mass and humidity as a function of time. The blue line represents the relative humidity and the red line is the net change in mass.

In Figure 3.11, Image B, it can be seen that the sample is first gaining and then losing weight under the same RH level, seen in the fourth step represented by the red line, which is an indication of solvent desorption from the particles. This process can also be seen in Image A when comparing the mass at the beginning of the sorption cycle at 20% with the mass after desorption at 20% RH. It can be seen that there is a weight loss which could partly be explained by the evaporation of the solvent. In image A, at the beginning of the process, the slope of the red line is not steep. However, as the relative humidity of the environment increases between 60-80%, the slope gets steeper. This is an identification of the sample absorbing more water at higher RH values as that the change in mass is relatively high for a given change in the relative humidity of the environment at that point. However, it is also a consequence from the release of solvent molecules which counteract the weight increase and provide apparently smaller steps. This process can also be seen in Image B, as the smaller steps at the beginning of the process get bigger as the RH reaches 80%.

During the desorption phase, the sample showed a gradual reduction in mass as the relative humidity was decreased, following a consistent pattern, seen in image B. This pattern can be observed as the size of the steps remains equal until reaching approximately 20% relative humidity, after which the step size increases. The results indicated that the rate of mass loss was higher at lower relative humidity conditions, indicating that the DSM-A had a less strong affinity for moisture and retained moisture at low RH. The same process can be seen in image A where the blue line, corresponding to the desorption process, followed a similar pattern, remaining flat until approximately 20% relative humidity, after which it became steeper, indicating an increased rate of mass loss by the sample. DSM-A is gaining in total 20% in mass at 80% RH relative to the 0% RH step during the whole analysis indicating that this DSM batch is good at absorbing moisture and thus is hygroscopic according to Table 3.5.

Table 3.5. Classification according to the European Pharmacopoeia Method (Per. Eur.).

Material category	Criteria as per Ph. Eur. *
NH	0-0.012% w/w
SH	0.2-2% w/w
MH	2-15% w/w
VH	More than 15% w/w

* Weight gain due to moisture sorption at 25 °C-80% RH. NH: Non-hygroscopic, SH: Slightly hygroscopic, MH: Moderately hygroscopic, VH: Very hygroscopic.

3.3.2 DSM-S

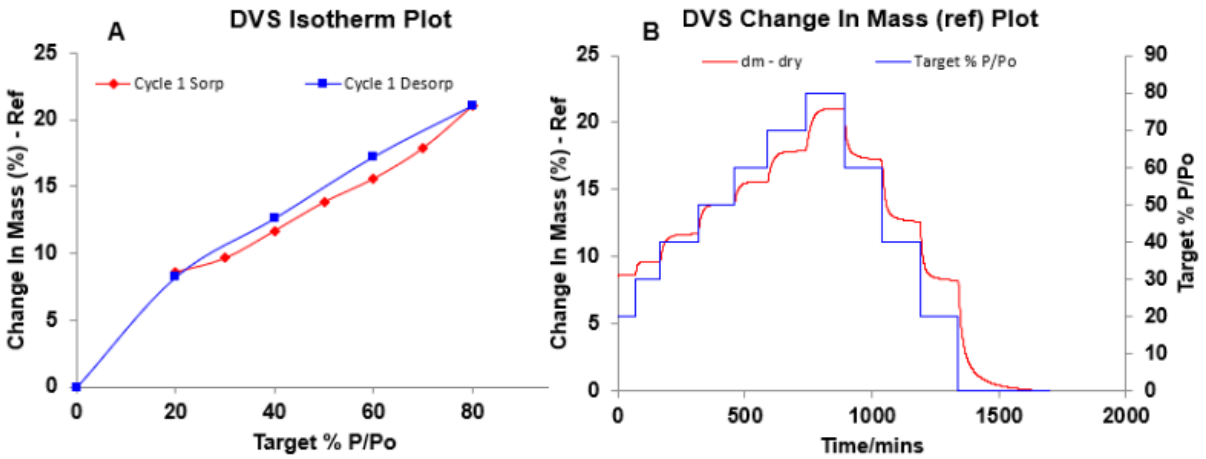

Figure 3.12. Displays the moisture interaction for DSM-S. In Image A, the relationship between mass and relative humidity is visualized, with the x-axis representing relative humidity and the y-axis representing mass. The blue line indicates desorption, while the red line represents absorption. Image B illustrates the variation of mass and humidity over time, with the blue line representing relative humidity and the red line indicating the net change in mass.

In Figure 3.12, Image A, the sorption line and the desorption line start at the same point and do not intersect throughout the process, indicating that no solvent is present. During the entire analysis, the desorption isotherm remains consistently above the sorption isotherm, showing that there is a difference in sorption and the desorption mechanism. As for DSM-A, this batch is having a slower moisture uptake at the beginning of the process which then increases, seen as the larger steps at the end. Also, the desorption phase follows the similar pattern as for DSM-A, indicating that this batch also has less strong affinity for moisture at lower RH values. Similarly to DSM-A, DSM-S gain in total approximately 20% in mass at 80% RH relative to the 0% RH step indicating that this batch is also highly hygroscopic.

3.3.3 DSM -T

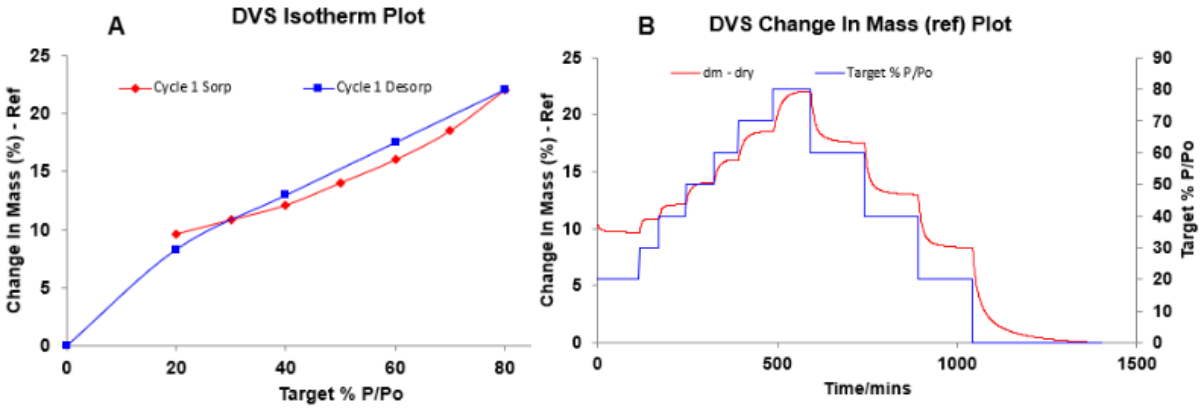

Figure 3.13: Displays the behavior of DSM-T under different RH levels. Image A depicts the correlation between mass and relative humidity, where the x-axis represents relative humidity, and the y-axis represents mass. The blue line shows the desorption, while the red line represents the absorption. In Image B, the change in mass and humidity over time is depicted, with the blue line representing relative humidity, and the red line showing the net change in mass.

Figure 3.13 represents the GVS analysis of DSM-T. In Image A, there is a difference in mass for the sorption and desorption isotherms at 20% RH where both lines don't intersect as for DSM-A. This indicates that this batch also has some solvent as for DSM-A. However, in this case, this can not be seen in Image B which may be due to DSM-T having another kinetic or tempo of desorbing and absorbing moisture. The behavior of DSM-T powder is similar to that of DSM-A and DSM-S batches. Like the previous batches, the DSM-T particles show a lower adsorption of moisture at lower relative humidity conditions that increases as the RH level is raised. The desorption phase also follows the same pattern as all DSM batches. Furthermore, the DSM-T sample gains approximately 20% in weight, which suggests that it is highly hygroscopic, as observed in the previous batches.

3.3.4 DSM-L

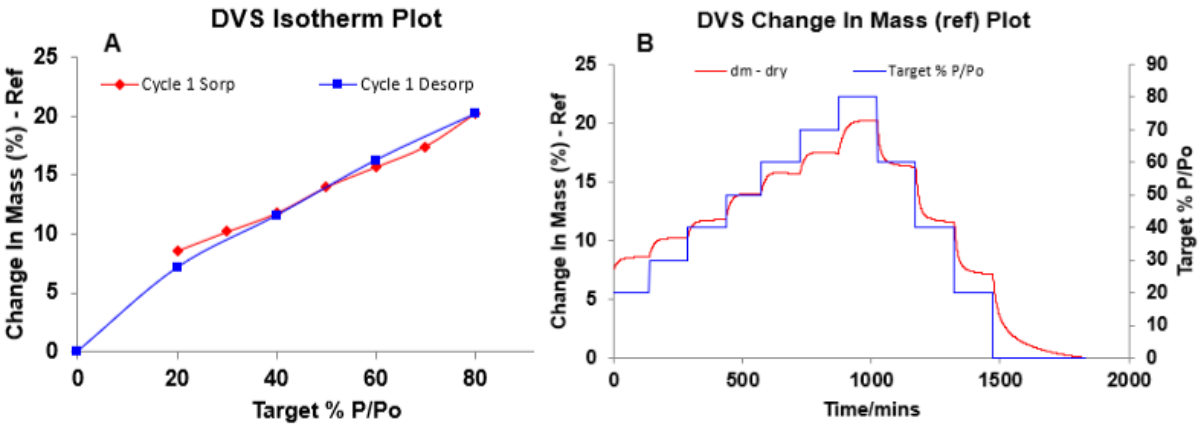

Figure 3.14: The response of DSM-L to various levels of relative humidity. Image A visualizes the relationship between mass and relative humidity, with the x-axis indicating relative humidity, and the y-axis indicating mass.

The blue line represents desorption, while the red line illustrates absorption. Image B displays the alteration of mass and humidity with time, with the blue line representing relative humidity, and the red line displaying the net change in mass.

Figure 3.14 shows the gravimetric vapor sorption analysis of DSM-L. Also, as for all other DSM batches, DSM-L also have a similar behavior as the RH is altered. The powder is also gaining approximately 20% in mass at 80% RH relative to the 0% RH step, indicating that this batch, as for the other ones, is also highly hygroscopic. The sorption and desorption isotherms in Image A intersect at approximately 40% RH and there is also for this batch a difference in mass for the sorption and desorption isotherms at 20%. This means that, as for the other batches, except for DSM-S, this batch also contains some solvent that is being removed from the spheres during the process. However, as for DSM-T, this can not clearly be seen in Image B which could be due to the properties of the spheres.

A conclusion could be drawn that all batches have a similar moisture interaction. According to the results, all DSM batches are expected to have faster moisture absorption at high RH but are overall highly hygroscopic. DMS-S is the only quality with no indications of residual solvents.

3.3.5 Nasaleze

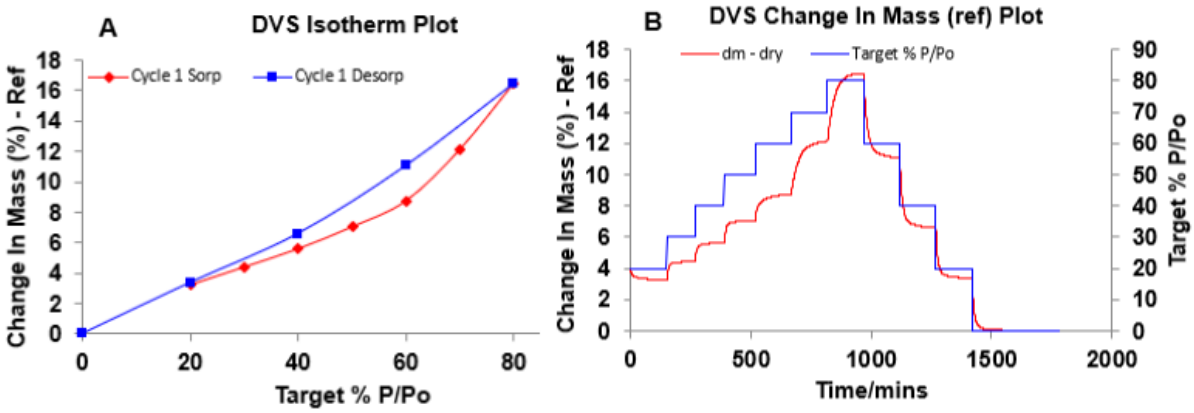

Figure 3.15. The moisture interaction of Nasaleze. Image A depicts the correlation between mass and relative humidity, where the x-axis represents relative humidity, and the y-axis represents mass. Desorption and absorption are indicated by the blue and red lines, respectively. In Image B, the changes in mass and humidity over time are presented, with the blue line representing relative humidity, and the red line showing the net change in mass.

The graphs in Figure 3.15 were generated from analyzing Nasaleze. Image A shows that the crossing point occurred at the beginning of the process at 20% RH, meaning that no solvent is present. In addition, the desorption line was consistently above the sorption line, indicating positive hysteresis throughout the process. The approximately same behavior was observed in DSM-S. However, in this case, the sorption line steepness increases after approximately 60%. Even though they have similar behavior, DSM-S have an overall lower hysteresis value than Nasaleze, see Appendix E.

According to the results, Nasaleze has the highest hysteresis amongst all batches indicating that it less efficiently releases the moisture compared to the DSM batches. The powder exhibits lower hygroscopicity than the DSM batches, due to the sample absorbing 16% in mass compared to the DSM batches that absorbed approximately 20%. However, according to Table 3.5, the sample is still classified as highly hygroscopic. This difference in behavior is due to the difference in material composition between Nasaleze and the DSM batches. These variances include unique surface structures, porosity, and chemical compositions, which impact the adsorbtion and desorption of water molecules. Surface structures and porosity affect water molecules accessibility and moisture release efficiency, while the chemical composition introduce distinct interactions with water molecules based on different functional groups. These factors collectively influence the sorbtion behavior of the samples.

3.4 BET

The BET analyses were performed on DSM-A, DSM-S, DSM-T and DSM-L. However, μ-pore analyses were only conducted on DSM-A. DSM-T and DSM-L had very low surface areas, making it impossible to analyze them accurately. Nevertheless, the μ-pore analysis for DSM-A and the BET analysis for DSM-A and DSM-S gave useful results, see Table 3.6.

Tabel 3.6. Shows the different parameters generated from the BET analysis of DSM-A and DSM-S.

Batch	**BET surface area (m^2/g)**	**C-value**	**micropore-area (m^2/g)**	**external surface-area (m^2/g)**
DSM-A	2.61	144.02	2.31	0.32
DSM-S	0.20	141.61	N/A	N/A

*NA: Not applicable.

DSM-A had a higher BET surface area of 2.61 m^2/g compared to DSM-S, which had a BET surface area of 0.2 m^2/g. This suggests that DSM-A may have a larger total pore volume or more extensive pore structure than DSM-S. The micropore analysis of DSM-A revealed that the material had a micropore area of 2.31 m^2/g, indicating a significant amount of micropores in the material.

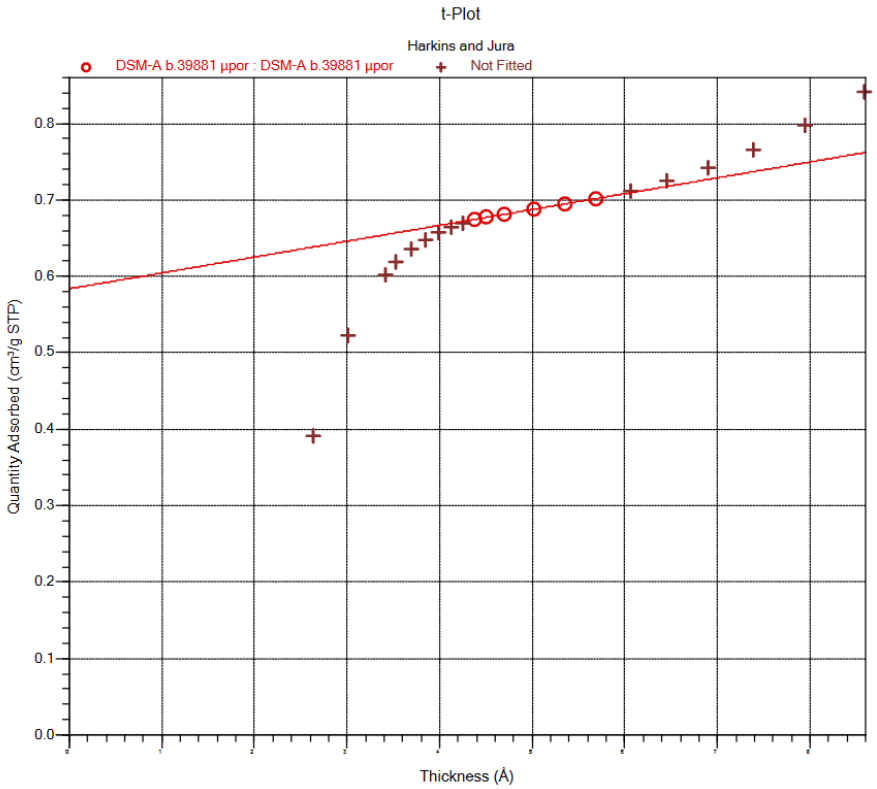

Figure 3.16. Generated t-plot from BET analysis of DSM-A. The Y-axis represents the quantity of gas adsorbed, while the X-axis displays the thickness of the adsorbed layer.

This can also be seen from the generated t-plot, see Figure 3.16, where a straight line would have been observed if there were no pores, as nitrogen absorption would increase linearly with layer thickness. However, the presence of micropores results in higher nitrogen uptake initially, followed by a decrease in the amount of nitrogen per layer as the pores become saturated. The external surface area was found to be 0.32 m^2/g, which is low compared to the total surface area (BET). This information suggests that the material has a high proportion of micropores and a relatively low external surface area indicating that most of the surface area comes from the pores.

The generated specific surface area from the PSD analyses, see Appendix A, differ a lot from the BET surface area for DSM-A, proving further that the largest contribution to the area are the internal micropores. However, for DSM-S, the values are quite similar, indicating a smooth structure.

The C value of DSM-A is slightly higher than that of DSM-S, with DSM-A having a C value of 144.0 and DSM-S having a C value of 141.6. However, the difference is not significant indicating that both particles exhibit approximately the same affinity for the adsorbate. This may be due to both having similar surface chemistry.

3.5 Bulk density

The bulk density for each batch was derived using the data presented in Appendix B. The calculated bulk density was plotted against the median particle size at 60% sonication and the resulting plot is shown in Figure 3.17.

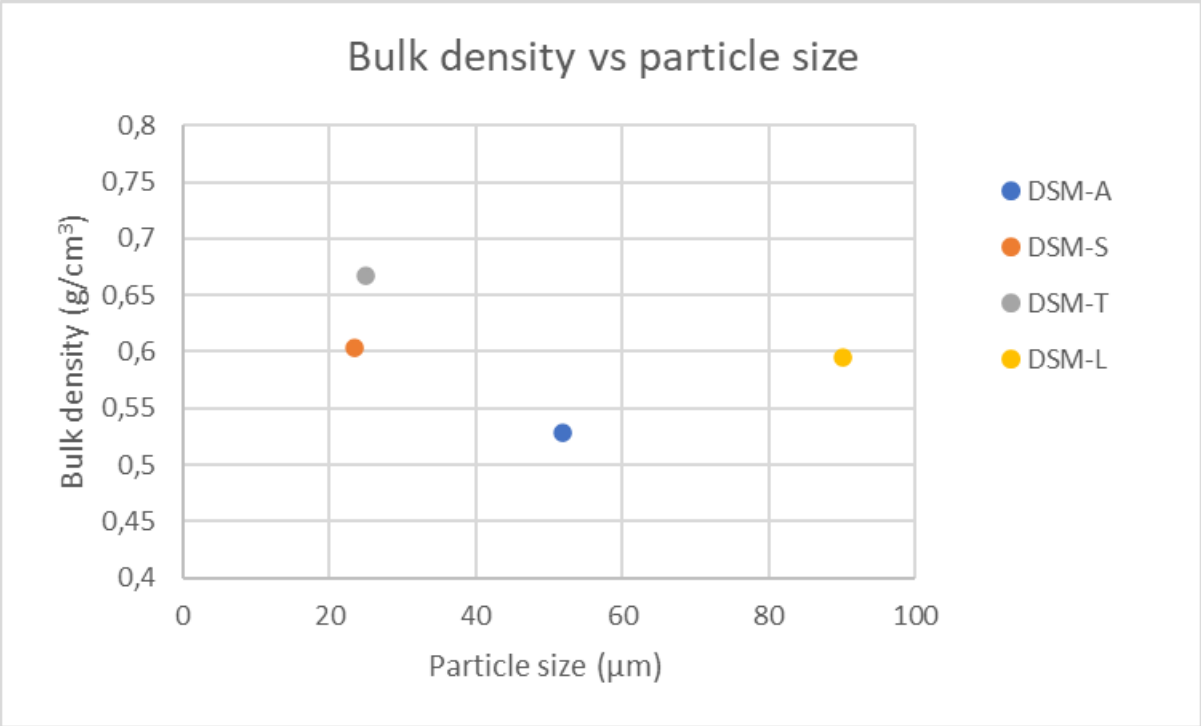

Figure 3.17: Displays a plot of the mean d50 particle size and the bulk density. The standard deviation was calculated to be a very low value and therefore not included in the figure.

The d50 particle sizes for DSM-S and DSM-T are similar. However, they exhibited different bulk densities with DSM-T (0.67 g/cm^3) having a higher bulk density than DSM-S (0.60 g/cm^3). This was expected since DSM-T exhibited a lower span value than DSM-S, see Table 3.1. A narrower particle size distribution allows for more efficient packing of particles, resulting in a higher bulk density. DSM-L (90.1 µm) with the highest particle size has a bulk density of 0.60 g/ cm^3 meaning that it has the same bulk density as DSM-S, which is probably due to the agglomerates present in DSM-L. DSM-A having the second biggest d50 value had the smallest bulk density of 0.53 g/cm^3. This means that DSM-A is less dense than the other batches which could be due the powder also exhibiting the lowest true density, see Table 3.6, but especially due to the particles having a wrinkled surface.

The results indicate that factors other than particle size may have a more substantial influence on bulk density. The absence of a consistent pattern between particle size and bulk density suggests that their relationship is not straightforward. It implies that other variables, such as the presence of agglomerates and the crinkliness of the surface, could play a crucial role in determining bulk density.

3.6 Packing density

The packing density of DSM-A, DSM-S, DSM-T and DSM-L were calculated using bulk density, see Appendix B and true density data, see Table 3.7.

Table 3.7: The derived true density for the different DSM batches

Sample	Density (g/ cm^3)
DSM-T	1.32
DSM-L	1.30
DSM-S	1.32
DSM-A	1.22

All batches, except for DSM-A, which had the lowest value of 1.22 g/ cm^3, showed similar true density values, see Table 3.7. The lower value of DSM-A could be due to the fact that the individual particles have a lower mass per unit volume compared to the other DSM batches. This suggests that the particles have a less compact internal structure.

The calculated packing density and mean particle size of each batch were plotted as a scatter plot in Figure 3.18.

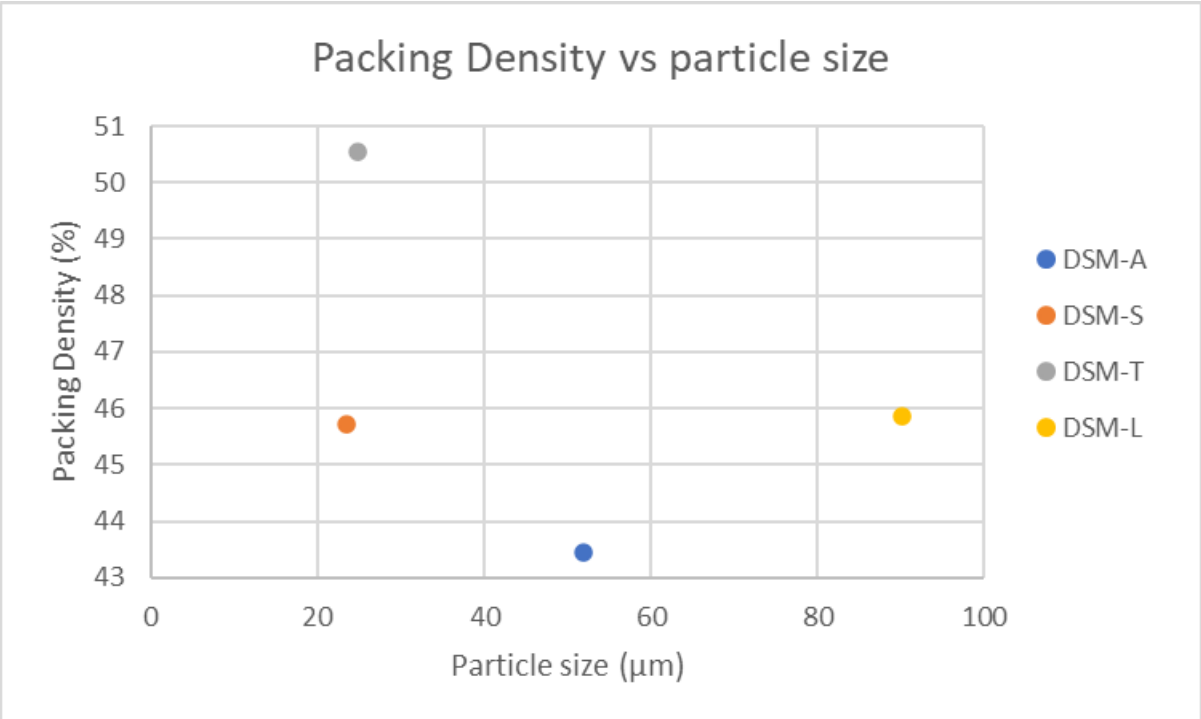

Figure 3.18. Displays the packing density of the different DSM batches. The blue dot represents DSM-A and orange plot DSM-S. DSM-T and DSM-L are represented by gray and yellow color respectively. The X-axis represents the particle size, while the Y-axis shows the packing density.

The results showed that DSM-T had the highest packing density (50.5%), followed by DSM-L (45.9%), DSM-S (45.7%), and DSM-A (43.5%). No correlation between particle size and packing density could be seen since all calculated packing densities are similar in value despite their differences in particle size. If a material has a high packing density, it indicates that the particles or components of the material are tightly packed together, resulting in a high mass per unit volume. The highest packing density of DSM-T could be due to the more uniform and narrow particle size distribution, indicating that there is minimal empty space or voids between the particles, leading to a more compact and dense structure. On the other hand, DSM-A had the lowest packing density, which could be due to the powder having a wider range of particle sizes and scrunchy surface structure of the spheres, leading to a more loosely packed powder. A powder with a low packing density may have better dispersibility, which also was observed in the PSD analysis for DSM-A, see Figure 3.4, which could be important for applications such as inhalation drug delivery.

3.7 Powder Flow (Angle of Repose)

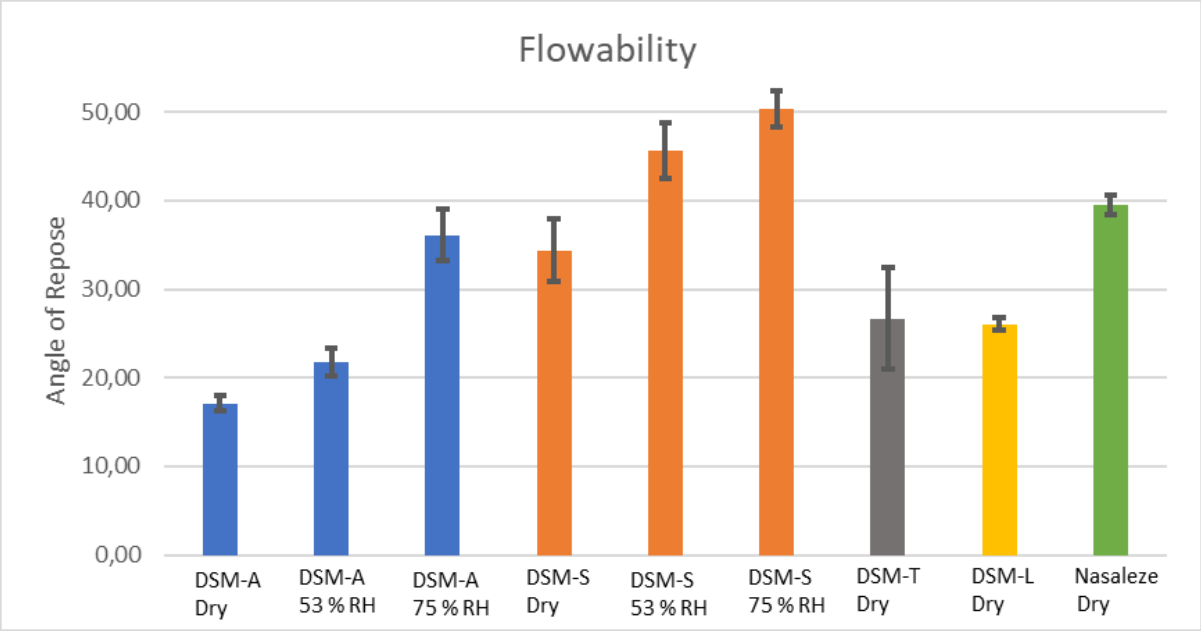

Figure 3.19: The staple diagram where each bar represents the angle of repose for a different batch of DSM. The height of each bar corresponds to the average angle of repose for the batch, while the error bars indicate the standard deviation.The blue bars represent the DSM-A sample stored under various conditions, while the orange bars represent the DSM-S samples stored under different conditions. The gray, yellow, and green bars correspond to DSM-T, DSM-L, and Nasaleze, respectively, all stored under dry conditions.

Figure 3.19 shows the angle of repose for the different DSM batches and the reference Nasaleze. The analysis was done on all four batches and Nasaleze at dry conditions and DSM-A and DSM-S were further analyzed at different RH (53% and 75%). The results indicate that there is a variation in the angle of repose between different batches of DSM at dry conditions. A high AOR indicates a poor fluency and vice versa. DSM-A stored under dry conditions had the lowest angle of repose, with an average of 17 degrees. This observation aligns with expectations, as DSM-A consists of particles that are less densely

packed and possess a less compact internal structure. DSM-T and DSM-L exhibited similar flowability with an angle of response value of 26. DSM-S got the highest angle of repose value of 34 amongst the batches stored under dry conditions, again pointing that this batch is the most cohesive one.

The same pattern for DSM-S and DSM-A stored under different RH conditions can be noted where the angle of repose is increasing (flowability is decreasing) with increasing RH. This was expected since, see Table 3.2 and 3.3, more agglomerates are being formed as the RH is raised. This in turn alters the cohesiveness of the powders and thus causes a reduction in the flowability of the powder.

Overall, these results indicate that the angle of repose increased as the RH increased, indicating that powders stored in higher RH values were more difficult to flow. When comparing all four batches stored in dry conditions, the findings suggest that the angle of repose is affected by variations in material properties.

The Pharmacopeia definitions (see Table 3.8) indicate that all batches stored under dry conditions, except for DSM-S, exhibit excellent flow properties whereas DSM-S demonstrates good flow properties. The flow properties remain excellent and good for DSM-A stored at 53% RH and 75% RH respectively. For DSM-S, the flow properties are considered to be passable and poor at RH 53% and 75% respectively. This indicates that as RH increases, DSM-S is more impacted in terms of flow properties compared to DSM-A,

The angle of repose for Nasaleze was measured to be 39 degrees, which is higher than all of the DSM batches at dry conditions, indicating that it has slightly poorer flow properties. This is obviously expected based on appearance, seen in Figure 3.3. According to Pharmacopoeia definitions, Nasalese have fair (aid not needed) flow properties.

Table 3.8. Flow properties and corresponding angles of repose

Flow property	Angle of repose (degrees)
Excellent	25-30
Good	31-35
Fair (aid not needed)	36-40
Passable (may hang up)	41-45
Poor (must agitate, vibrate)	46-55
Very poor	56-65
Very, very poor	> 66

*European Pharmacopoeia: EP 2.9.36

3.8 SprayTec

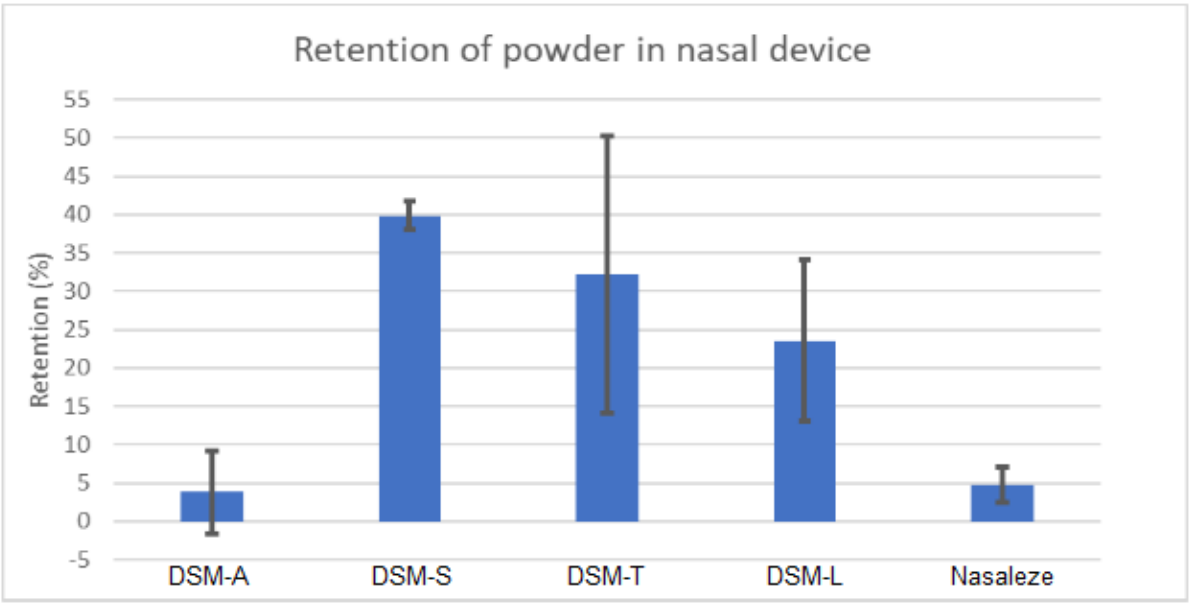

Figure 3.19. Calculated retention and standard deviation of the nasal devices whose cavity only was filled with approximately 50% of the different batches of DSM and Nasaleze stored under dry conditions.

The results of analyzing the ICOone device at 30 L/min, where 50% of the nasal cavity was filled with the different DSM batches and Nasaleze is displayed in Figure 3.19. Among the tested batches, DSM-A showed the lowest retention value, indicating that it was the easiest to empty from the device. The value was almost zero, suggesting that almost all powder was emptied at a flow rate of 30 L/min. However, due to the high variability a high standard deviation value was calculated, shown by the error bar. This was due to the retention value being calculated as zero for all devices, except for one that had a slightly higher value, see Appendix. Notably, the retention value of DSM-A was similar to that calculated from Nasaleze. In contrast, the retention values for the other DSM batches were higher, indicating that less powder was emptied from the device. Among the tested batches, DSM-S exhibited the worst retention behavior, showing the highest retention value. These findings suggest that the retention behavior of the DSM powder batches varied and could impact their effectiveness when administered via a nasal device.

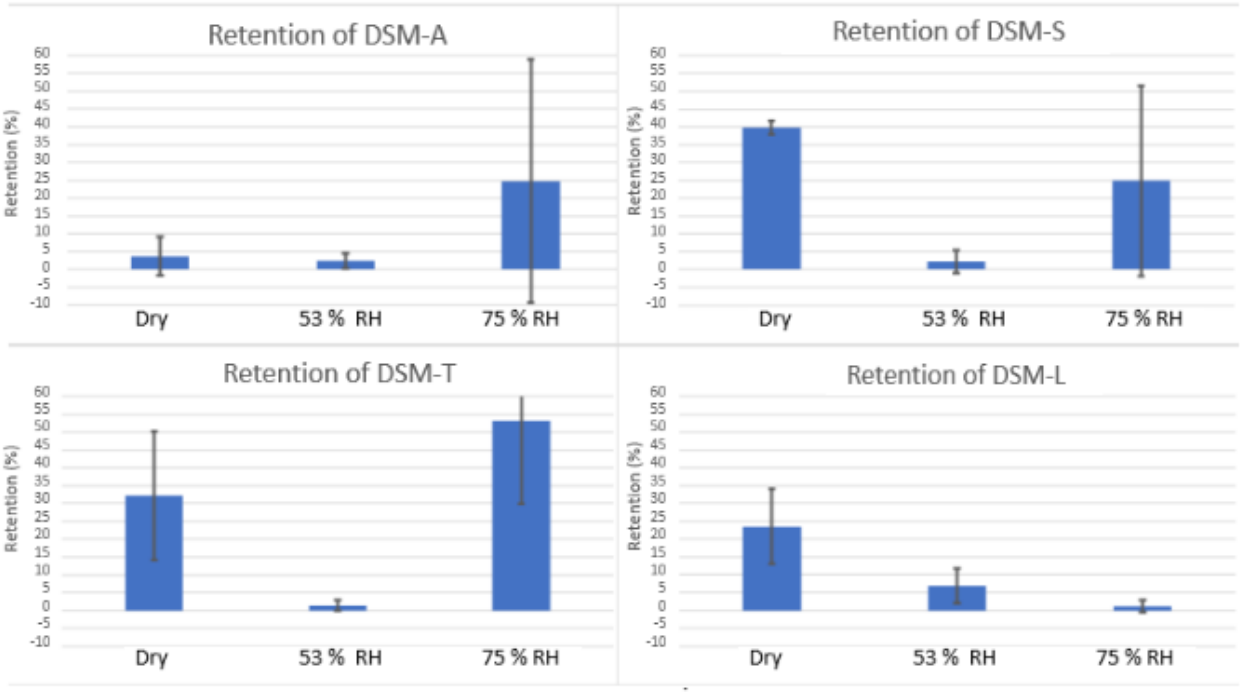

Figure 3.20. Calculated retention value of the ICOone device filled with the different DSM batches stored under different RH values.

Based on the results obtained, it can be observed that the retention behavior of the four different powder batches from the ICOone device were affected by the RH levels at which they were tested, see Figure 3.20. The retention value for DSM-A was consistent at both dry conditions and 53% RH. However, at 75% RH, the retention value for DSM-A was higher, indicating that less powder was emptied at this higher humidity level. This could be due to the reduced flowability of the powder at the higher RH value as seen in Figure 3.19.

In contrast, DSM-S and DSM-T did not follow this pattern. For these batches, retention decreased as RH level increased to 53%, but then increased again at 75% RH. However, as seen in Figure 3.9, the flowability of DSM-S reduces at higher RH values. Nevertheless, the reason for the lower retention value at 53% RH compared to dry conditions could be due to electrostatic forces between the particles that can promote particle-device adhesion.

Finally, DSM-L showed the opposite pattern to DSM-A, with retention decreasing as RH level increased. In this case, the moisture could have a disruptive effect on the particle-device interactions, as for DSM-S and DSM-T at 53% RH, reducing the adhesion and increasing the ease of powder release from the device. These results suggest that the different DSM powders have varying properties that affect their retention behavior under different humidity conditions.

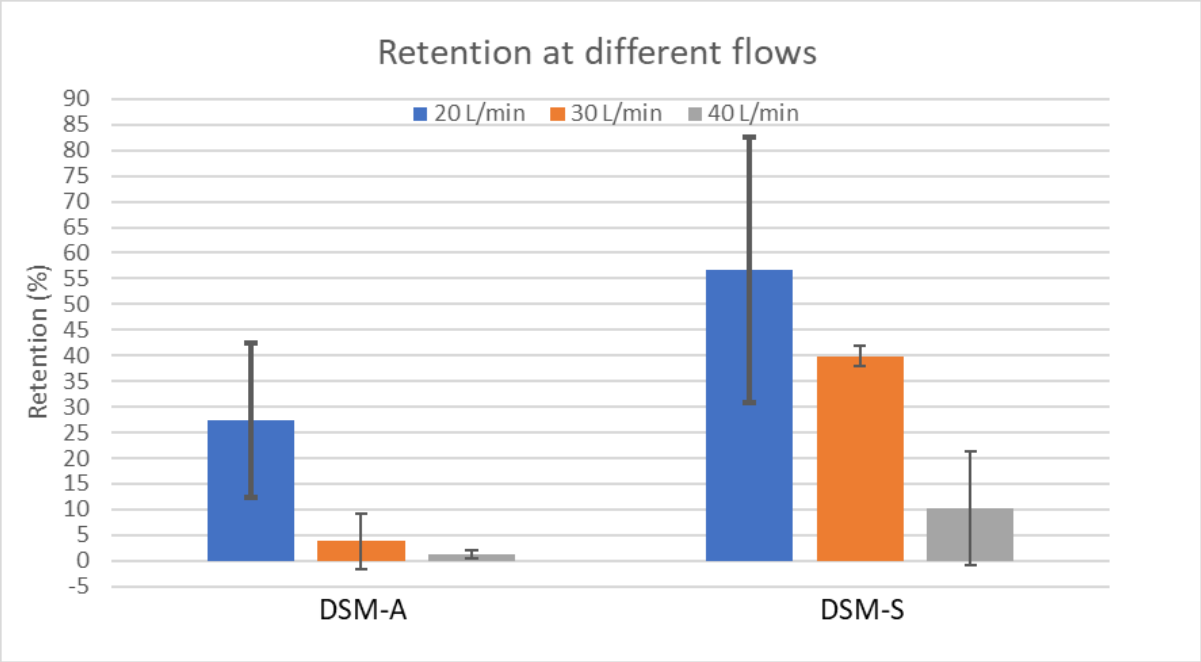

Figure 3.21. Retention value of DSM-A and DSM-S tested at different flow rates of 20, 30 and 40 L/min. The error bars indicate the variation the retention value.

Figure 3.21 displays the retention analysis performed at different flow rates on DSM-A and DSM-S, stored under dry conditions The results showed that the retention value decreased for both powders as the flow rate increased. Higher flow rates can cause more turbulence in the device, leading to less powder retention. For DSM-A, the retention was very close to zero at both 30 L/min and 40 L/min, indicating that this batch is independent of flow rates above 30 L/min. On the other hand, DSM-S never reached zero but decreased to a minimum of 10% at 40 L/min. These results suggest that the flow rate has a impact on the retention of powders in nasal devices.

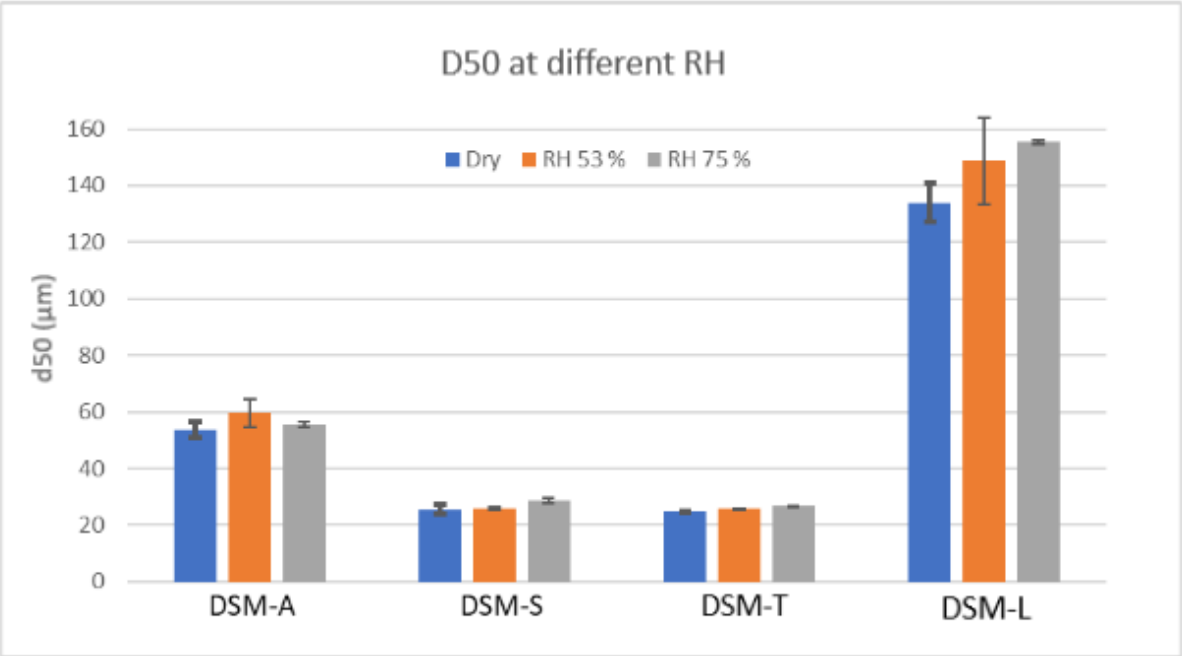

Figure 3.21. The mean particle size value of the different DSM batches stored under various RH levels of dry, 53% and 75%. The error bars represents the standard deviation value.

The d50 value remained relatively constant across all batches, see Figure 3.21, except for DSM-L, which showed some variation with changes in the RH value. Despite this, the change in d50 value for DSM-L was not significant, with values ranging from 134.03-155.35 µm. The results are consistent with the PSD analysis results presented in Table 3.1, except for DSM-L that got a significantly higher d50 value in the SprayTec analysis compared to the PSD analysis. This is due to the ICOone device not having as good deaggregation ability as the Malvern mastersizer equipment.

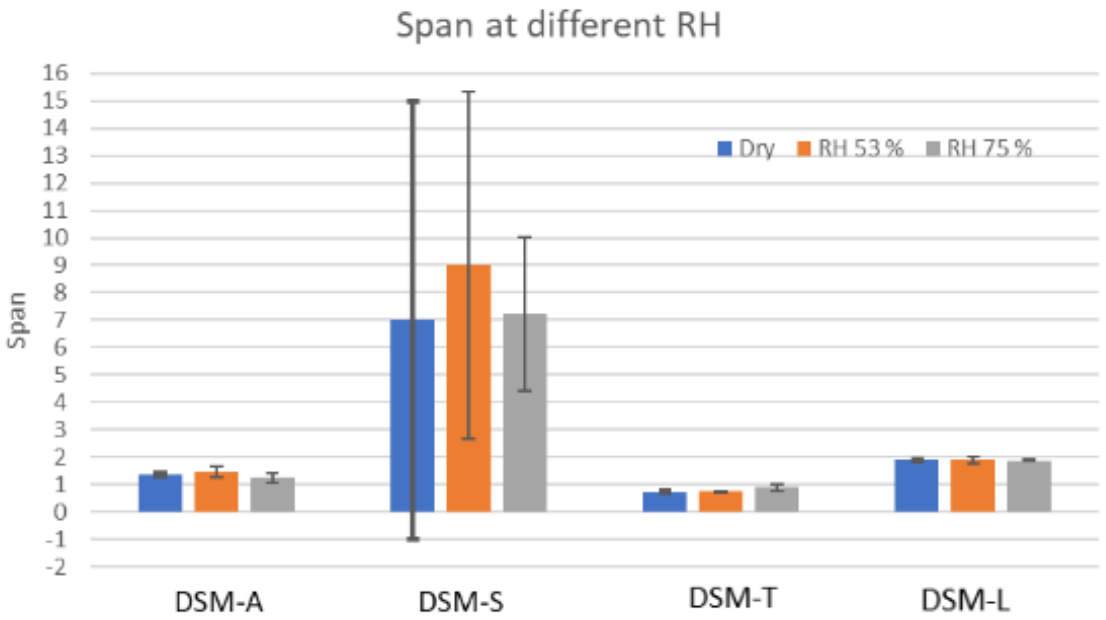

Figure 3.22. The span value of the different DSM batches stored under various RH levels of dry, 53% and 75%. The error bars indicate the standard deviation value.

The span values for all batches, except for DSM-S, showed consistency across different RH conditions and exhibited lower variation, as indicated by smaller error bars displayed in Figure 3.22. However, DSM-S showed larger variations in span values between different RH levels and within the same conditions. This behavior could be attributed to its tendency to form agglomerates. The PSD analysis in Figure 3.4 confirms this observation, as a higher sonication power was required to break down the agglomerates, indicating stronger interparticle adhesion forces. The significant variation in span values for DSM-S may be due to the formation of agglomerates, which can affect the particle size distribution and lead to a wider span value. On the other hand, the other powders may have exhibited less agglomeration and hence showed consistent span values across different RH conditions.

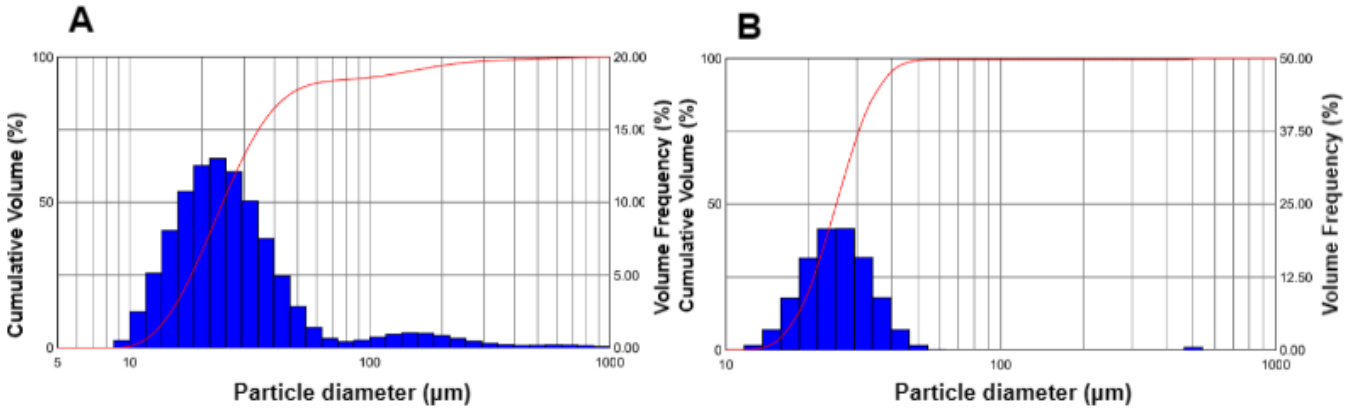

Figure 3.23. Particle size distribution curve of DSM-S, seen in image A, and DSM-T, seen in image B.

Figure 3.23 shows the average particle size distribution graph of DSM-S, Image A, and DSM-T, Image B. For DSM-S, a small peak after the main peak is present which is attributed

to the formation of agglomerates. This peak is not observed for DSM-T nor the other DSM batches. However, only comparison with DSM-T is made due to them both having similar particle sizes. The formation of agglomerate could be expected since the results from the PSD analysis indicated that DSM-S is the batch with the highest cohesiveness due to the particles having stronger interparticular forces, see Figure 3.4. Therefore, DSM-S exhibited a higher variation in the span value and big error bars.

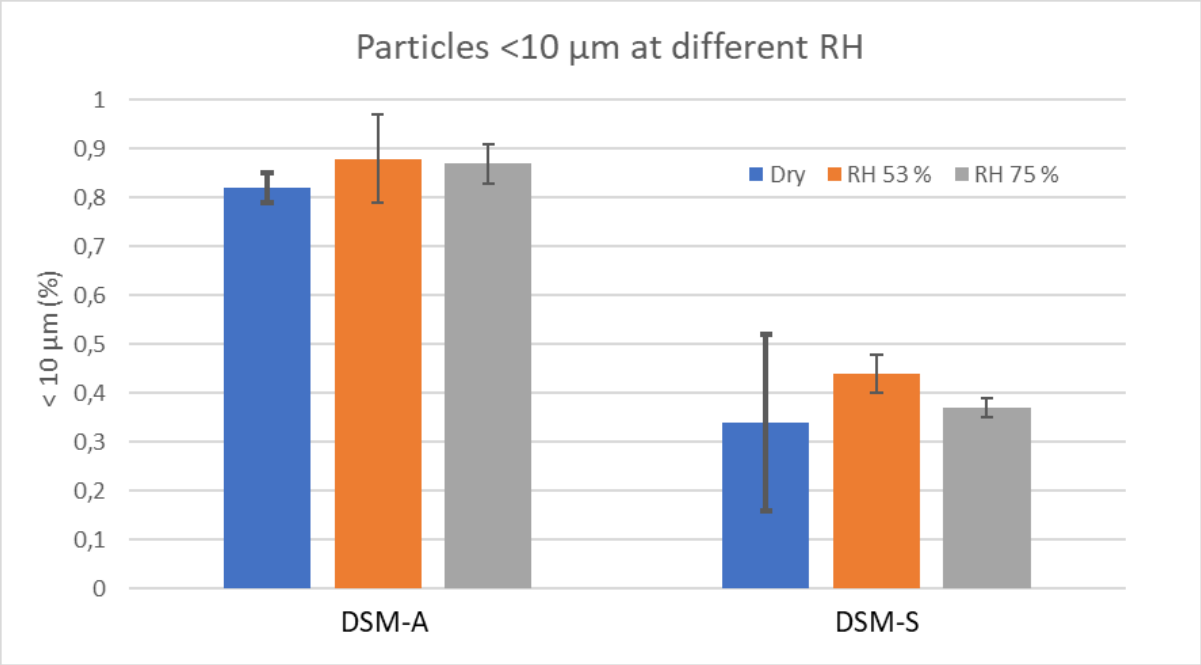

Figure 3.24. The percentage of particles under 10 microns for DSM-A and DSM-S stored at different RH levels, namely dry, 53% and 75%. The error bars represents the standard deviation value.

Figure 3.24 shows the percent of particles below 10 µm for DSM-A and DSM-S. The results generated from analyzing DSM-T and DSM-L are not included due to them both getting a value of zero. However, DSM-A exhibited the highest value ranging from 0,82-0,87. This is expected since DSM-A is less cohesive than DSM-S, resulting in a higher value. However, the value for both DSM-A and DSM-S is still very low indicating that a very low amount of particles will reach lower airways. A vast majority of the powder will be deposited in the nasal cavity, minimizing the risk of unintended lung deposition.

3.9 Nasal cast analysis

3.9.1 DSM-A

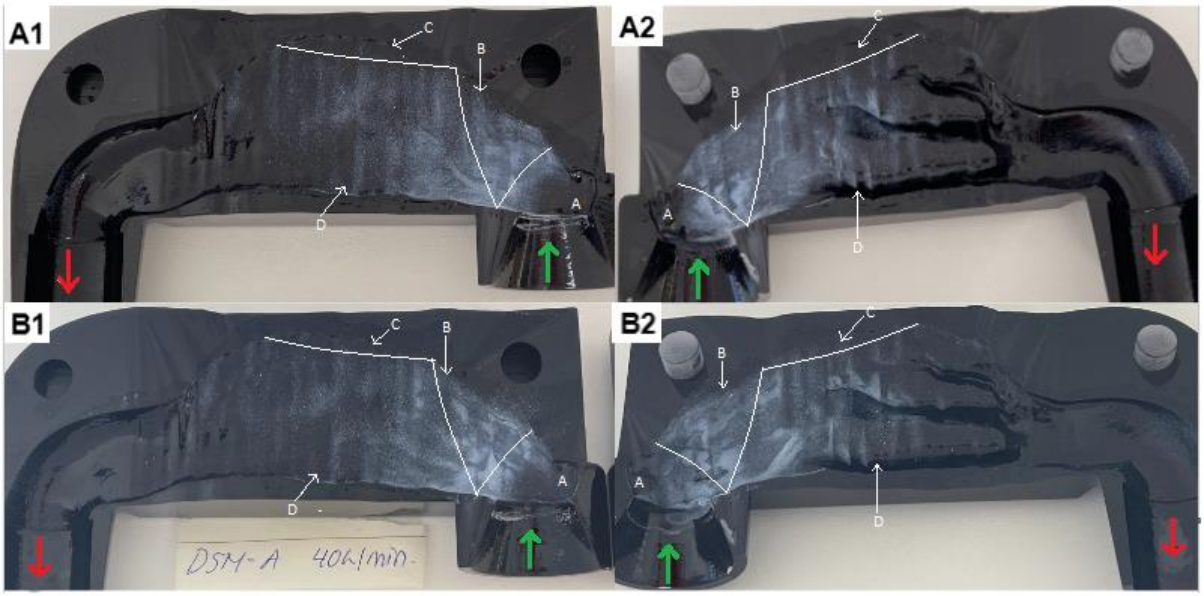

Figure 3.25. A sagittal section of the nasal cavity displaying the deposition profile of DSM-A. Image A1 and A2 correspond to analysis at 30 L/min. Image B1 and B2 corresponds to analysis at 40 L/min. The nostrils, serving as the inlet to the nasal cavity, are indicated by the green line, while the nasopharynx, serving as the outlet of the nasal cavity, is marked by the red line. The various regions within the nasal cavity, namely the nasal vestibule (A), atrium (B), olfactory region (C), and respiratory region (D), are approximately divided to indicate their respective locations.

Figure 3.25 shows the deposition profile of DSM-A stored in dry conditions at 30 and 40 L/min. The results indicate that the powder has an evenly spread distribution with no evidence of agglomerates. Additionally, DSM-A shows a similar deposition profile regardless of the flow rate. The majority of the powder adheres to the nasal vestibule and atrium area, while a significant amount reaches the respiratory region. However, the amount of powder observed in the olfactory region is either nonexistent or very low.

The results in Table 3.9 indicates that all powder at both flow rates emptied completely giving a retention value of zero.

Table 3.9. The calculated filling weight and retention value of DSM-A in the ICOone device.

Flow (L/min)	Fill weight (mg)	Retention (%)
30	34.7	0.0
30	15.2	0.0
30	21.2	0.0
40	25.5	0.0
40	25.9	0.0
40	28.0	0.0

3.9.2 DSM-S

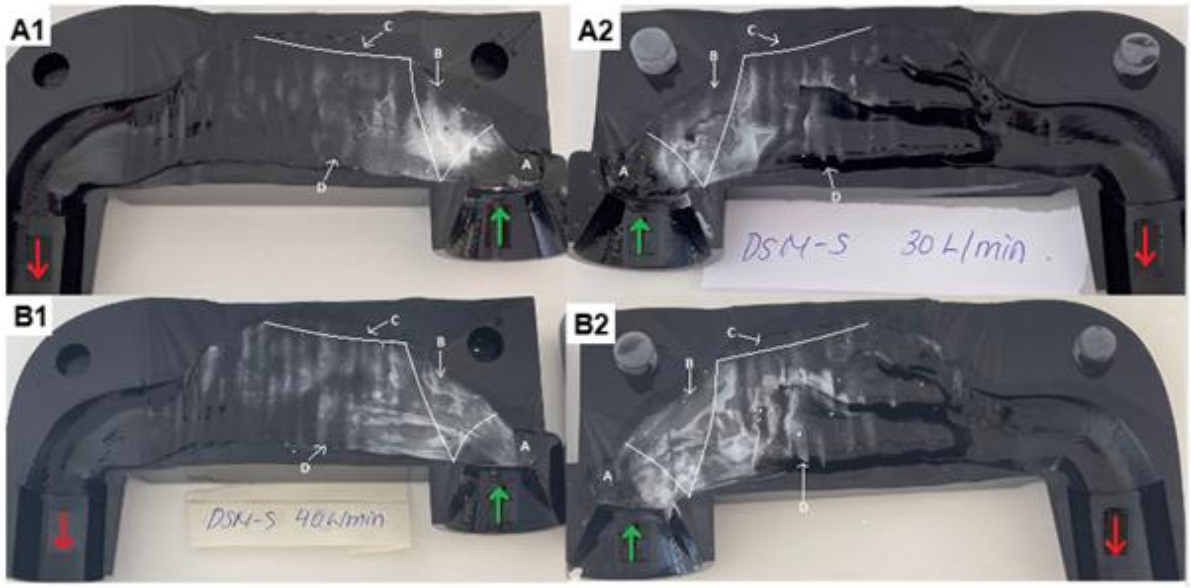

Figure 3.26. A sagittal section of the nasal cavity displaying the deposition profile of DSM-S. Image A1 and A2 correspond to analysis at 30 L/min. Image B1 and B2 corresponds to analysis at 40 L/min. The nostrils, serving as the inlet to the nasal cavity, are indicated by the green line, while the nasopharynx, serving as the outlet of the nasal cavity, is marked by the red line. The various regions within the nasal cavity, namely the nasal vestibule (A), atrium (B), olfactory region (C), and respiratory region (D), are approximately divided to indicate their respective locations.

Figure 3.26 shows the deposition profile of DSM-S powder that was stored under dry conditions. The results suggest that the deposition profile is affected by the flow rate used. At a lower flow rate of 30 L/min, the majority of the powder is deposited at the beginning of the cavity resulting in a high concentration in the vestibule area and atrium area. At a flow rate of 30 L/min, a certain amount of powder adheres to the respiratory region. However, at a flow rate of 40 L/min, the powder is distributed further into the nasal cavity. There is either no detectable powder or a minimal amount observed in the olfactory region. It is also observed that there are agglomerates present, at both flow rates, which result in a high local concentration and delayed dissolution. This could have negative effects such as the occurrence of local toxic effects or reactions if the DSM spheres were loaded with API.

The results in Table 3.10 show that the powder was not fully emptied at either of the two tested flow rates. Nevertheless, the retention value decreases with an increase in flow rate. The results indicate a high variability with regard to emptying, similar to the results from Spraytec analysis in Figure 3.21.

Table 3.10. The determined filling weight and retention value of DSM-S in the ICOone device.

Flow (L/min)	Fill weight (mg)	Retention (%)
30	26.4	52.3
30	25.1	42.2
30	18.7	1.1
40	25.4	12.6
40	32.9	0.0
40	26.2	2.7

3.9.3 DSM-T

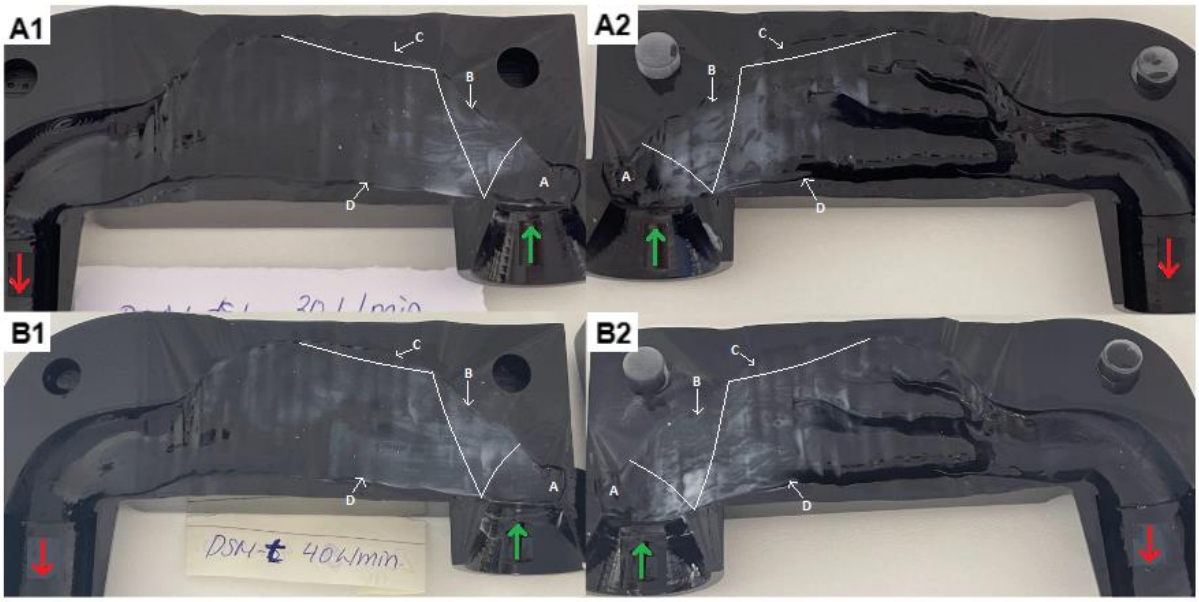

Figure 3.27. A sagittal section of the nasal cavity displaying the deposition profile of DSM-T. Image A1 and A2 correspond to analysis at 30 L/min. Image B1 and B2 corresponds to analysis at 40 L/min. The nostrils, serving as the inlet to the nasal cavity, are indicated by the green line, while the nasopharynx, serving as the outlet of the nasal cavity, is marked by the red line. The various regions within the nasal cavity, namely the nasal vestibule (A), atrium (B), olfactory region (C), and respiratory region (D), are approximately divided to indicate their respective locations.

The deposition profile of DSM-T appears less distinct compared to the other batches, see Figure 3.27. The less distinct deposition profile of DSM-T could be due to the powder forming a more gel-like structure faster in the lubricant than the other powders, which may have caused the less visible particles. The deposition profile of DSM-T is similar to DSM-S, with the majority of the powder adhering to the nasal vestibule and atrium areas at the beginning of the nasal cavity. However, at 40 L/min, the deposition expands to cover a larger area of the respiratory region, indicating a dependence on the flow rate. This can also be seen in Table 3.10, where the retention value decreases with increasing flow rate. Also, in this case, no visible particles are observed in the olfactory region and, as for DSM-A, there are no visible agglomerates.

Table 3.11 The determined weight of DSM-T during the filling process and the corresponding retention value in the ICOone device.

Flow (L/min)	Fill weight (mg)	Retention (%)
30	30.6	45.4
30	22.8	29.8
30	30.6	48.7
40	32.6	20.6
40	40.6	37.4
40	53.6	0.0

3.9.4 DSM-L

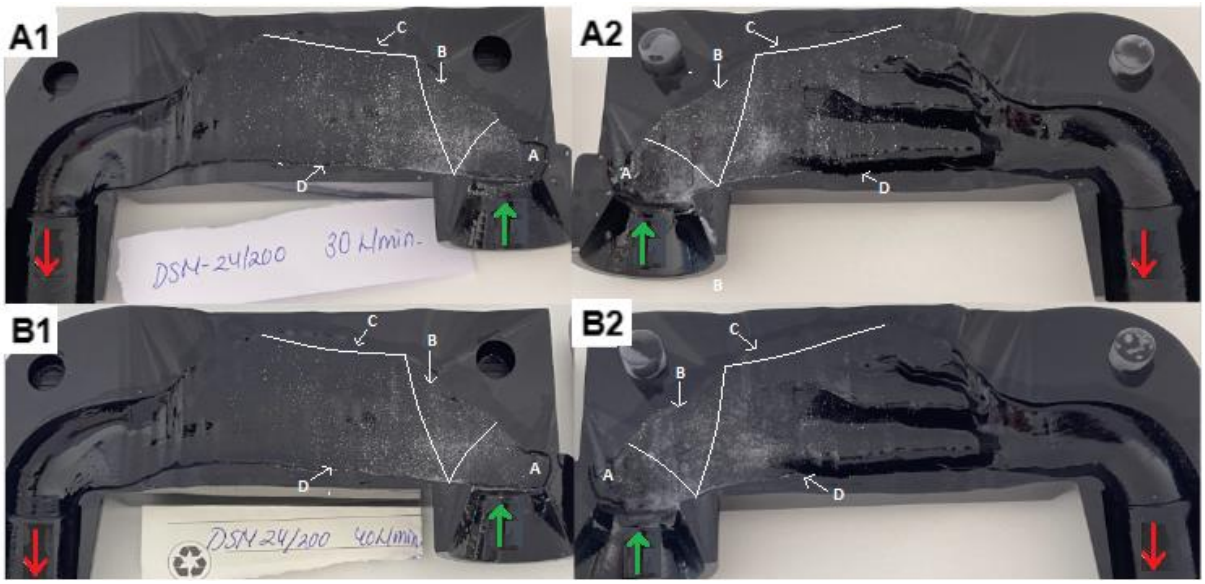

Figure 3.28. A sagittal cross-section of the nasal cavity displaying the deposition profile of DSM-L. Image A1 and A2 correspond to analysis at 30 L/min. Image B1 and B2 corresponds to analysis at 40 L/min. The nostrils, serving as the inlet to the nasal cavity, are indicated by the green line, while the nasopharynx, serving as the outlet of the nasal cavity, is marked by the red line. The various regions within the nasal cavity, namely the

nasal vestibule (A), atrium (B), olfactory region (C), and respiratory region (D), are approximately divided to indicate their respective locations.

The deposition profiles of DSM-L are displayed in Figure 3.28. The deposition profile of DSM-L, as in the case of DSM-A, remains consistent across different flow rates. However, in the case of DSM-L, the relatively larger particle size makes it easier to observe individual spheres compared to the other batches. As with the other powders, the majority of the powder is deposited at the beginning of the cavity, namely the nasal vestibule and atrium area. However, for DSM-L, a small amount has also deposited further into the nasal cavity covering a part of the respiratory region. As for the other DSM batches, no visible particles can be observed in the olfactory region. Also, in this case there are no visible agglomerates that were only present for DSM-S.

Table 3.12. The calculated filling weight and retention value of DSM-L in the ICOone device.

Flow (L/min)	Fill weight (mg)	Retention (%)
30	51.7	12.0
30	31.0	0.0
30	43.3	11.1
40	45.0	7.8
40	25.7	0.0
40	17.3	0.0

Table 3.11 shows that as the flow rate increases, the amount of powder retained in the ICOone device decreases. However, the results are quite variable, which is also reflected in the Spraytec analysis shown in Figures 3.19 and 3.20 where the error bars are quite large.

As seen in Table 3.12, there is a huge variation across the different doses analyzed at the same flow rate. This is consistent for all DSM batches, except for DSM-A in nasal cast analysis, see Table 3.9-10. This can also be observed by the big error bars in all figures generated from SprayTec analysis. One reason for this may be due to filling technique. Some devices may have been more compacted than others, resulting in a higher retention value. However, there is no correlation in the filling volume and retention value seen in Table 3.9-12 and Appendix F. Therefore, in order to draw any credible conclusions, further analyzes must be done.

3.9.5 Nasaleze

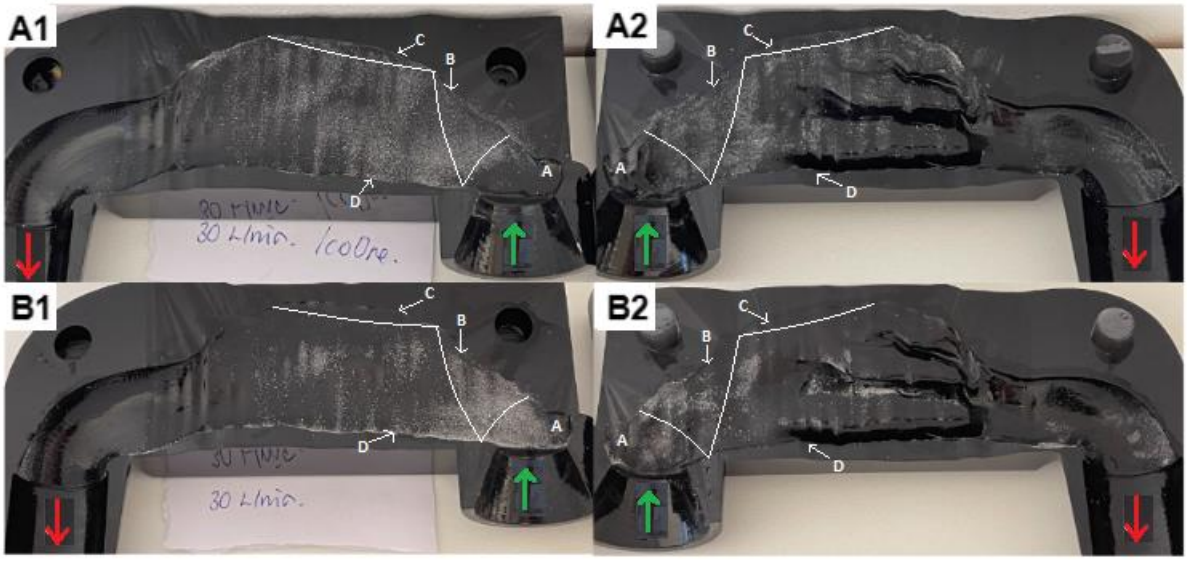

Figure 3.29. A sagittal section of the nasal cavity displaying the deposition profile of Nasaleze at a flow rate of 30 L/min. Images A1 and A2 correspond to analysis of Nasaleze in the ICOone device. Image B1 and B2 corresponds to analysis of Nasaleze in its original package (nasal spray pump). The nostrils, serving as the inlet to the nasal cavity, are indicated by the green line, while the nasopharynx, serving as the outlet of the nasal cavity, is marked by the red line. The various regions within the nasal cavity, namely the nasal vestibule (A), atrium (B), olfactory region (C), and respiratory region (D), are approximately divided to indicate their respective locations.

When using the ICOone nasal device, Nasaleze shows an evenly scattered deposition profile without any noticeable agglomerates throughout the nasal cavity, see Figure 3.29. However, when a nasal spray pump is used as the delivery device, the distribution of powder is uneven, with some areas having higher concentrations of powder than others. Despite this uneven distribution, the powder still reaches further into the nasal cavity, though the majority of it remains at the beginning of the cavity at the nasal vestibule and atrium area, which is consistent with the deposition profiles of the DSM batches. While the nasal spray pump only disperses the powder into the respiratory tract, using ICOone also allows the powder to reach the olfactory region.

4 Conclusions

The analysis of physical characteristics revealed that all DSM batches, except for DSM-A which possessed a distinct scrunchy structure, exhibit smooth surfaces. The surface structure of DSM-A contributed to its lower bulk density and packing density compared to all other DSM batches. Moreover, DSM-A had the lowest true density value and consisted of easily dispersible particles that were resistant to agglomeration. Conversely, the remaining DSM batches had a tendency to form agglomerates, with DSM-S exhibiting the highest level of cohesion. As a result, DSM-A demonstrated the highest flowability and DSM-S lowest, however, all batches exhibited good flow properties when stored under dry conditions.

The BET analysis revealed that DSM-A consisted of a significant amount of micropores compared to DSM-S that has a smooth structure. Furthermore, all DSM batches demonstrate high hygroscopicity, however, the particle size of DSM-A and DSM-S spheres shows limited sensitivity to changes in RH during storage.

The performance testing using SprayTec and nasal cast revealed that DSM-A demonstrates favorable retention behavior when used with the ICOone Nasal device, while DSM-S exhibits the poorest retention behavior. Nasal cast investigations demonstrate that all DSM batches exhibit adherence to the initial portion of the nasal cavity, namely the nasal vestibule and atrium area. Additionally, some particles from the DSM batches can distribute deeper into the respiratory region of the nasal cavity. DSM-A exhibits a deposition profile with a more uniform distribution, whereas DSM-S demonstrates visible agglomerates in its deposition profile. Nevertheless, none of the DSM batches reach the olfactory region compared to Nasaleze powder when used in the ICOone Nasal device, which covers all regions within the nasal cavity and exhibits an even distribution.

Finally, the ICOone Nasal device contributed to a good deposition profile covering a larger part of the nasal cavity compared to the Nasaleze nasal spray pump device. However, there was a large variation between the amount of powder retained between each dose when analyzed in the ICOone Nasal device which could be due to the filling technique used.

In conclusion, the analysis of the different DSM batches, namely DSM-A, DSM-S, DSM-T and DSM-L, and with the comparison to Nasaleze provides valuable insights into their suitability as nasal drug formulations. Amongst the DSM batches, DSM-A emerges as the most favorable choice for a nasal drug product and DSM-S as the least.

5 Future aspects

The powder deposition in the different regions within the nasal cavity was observed in this study through visual observation. However, quantification of deposition patterns could be conducted to determine the proportion of powder deposited in each region.
Furthermore, conducting an in vitro mucoadhesion test could assess the effectiveness of the spheres in adhering to the nasal mucosa. Lastly, considering the promising properties of DSM-A, further analysis could be done where these spheres could be loaded with a drug.

6 References

[1] S. Grassin-Delyle et al., "Intranasal drug delivery: an efficient and non-invasive route for systemic administration: focus on opioids," Pharmacol. Ther., vol. 134, no. 3, pp. 366-379, Jun. 2012. doi: 10.1016/j.pharmthera.2012.03.003.

[2] P. Henriques, A. Fortuna, and S. Doktorovová, "Spray dried powders for nasal delivery: Process and formulation considerations," Eur. J. Pharm. Biopharm., vol. 176, pp. 1-20, 2022. doi: 10.1016/j.ejpb.2022.05.002.

[3] T. Lapidot, M. Bouhajib, J. Faulknor, S. Khan, G.T. Krayz, C. Abrutzky, and D. Megiddo, "A Novel Faster-Acting, Dry Powder-Based, Naloxone Intranasal Formulation for Opioid Overdose," Pharm. Res., vol. 39, no. 5, pp. 963-975, May 2022. doi: 10.1007/s11095-022-03247-5.

[4] A. Pires, A. Fortuna, G. Alves, and A. Falcão, "Intranasal drug delivery: how, why and what for?" J. Pharm. Pharm. Sci., vol. 12, no. 3, pp. 288-311, 2009. doi: 10.18433/j3nc79.

[5] M. BaharAli, "Anatomy of the Nose," presented at SlideShare, SurgicoMed.com, Jun. 7, 2015. [Online]. Available: https://www.slideshare.net/MukhdoomBaharAli/anatomy-of-the-nose-surgicomedcom

[6] C. E. Nigro, J. F. Nigro, O. Mion, and J. F. Mello Jr., "Nasal valve: anatomy and physiology," Braz J Otorhinolaryngol, vol. 75, no. 2, pp. 305-310, Mar-Apr, 2009. doi: 10.1016/s1808-8694(15)30795-3. PMID: 19575121; PMCID: PMC9450767.

[7] P. S. Jorge, "Drug Absorption through the Nasal Mucosa: Current Challenges," Final Master's Thesis, Faculdade de Farmácia, Universidade de Lisboa, Lisbon, Portugal, 2021.

[8] M. I. Ugwoke et al., "The biopharmaceutical aspects of nasal mucoadhesive drug delivery," J. Pharm. Pharmacol., vol. 53, no. 1, pp. 3-21, Jan. 2001. doi: 10.1211/0022357011775145.

[9] Anatomy and Physiology of the Nasal Cavity (Inner Nose) and Mucosa," Virtual Medical Centre. [Online]. Available: https://www.myvmc.com/medical-centres/lungs-breathing/anatomy-and-physiology-of-the-nasal-cavity-inner-nose-and-mucosa/. [Acssesed: 27 Feb, 2023]

[10] C. R. Chen et al., "Anatomy and cellular constituents of the human olfactory mucosa: a review," J. Neurol. Surg. B Skull Base, vol. 75, no. 5, pp. 293-300, 2014. doi: 10.1055/s-0033-1361837.

[11] X. M. Bustamante-Marin and L. E. Ostrowski, "Cilia and Mucociliary Clearance," Cold Spring Harb. Perspect. Biol., vol. 9, no. 4, p. a028241, 2017. doi: 10.1101/cshperspect.a028241.

[12] L. Illum, "Nasal drug delivery—possibilities, problems and solutions," J. Control. Release, vol. 87, no. 1-3, pp. 187-198, 2003. doi: 10.1016/S0168-3659(02)00363-2.

[13] C. Rigaut, L. Deruyver, J. Goole, B. Haut, and P. Lambert, "Instillation of a Dry Powder in Nasal Casts: Parameters Influencing the Olfactory Deposition With Uni- and Bi-Directional Devices," Front. Med. Technol., vol. 4, p. 924501, Jun. 27, 2022. doi: 10.3389/fmedt.2022.924501. PMID: 35832236; PMCID: PMC9273033.

[14] B. M. Boddupalli et al., "Mucoadhesive drug delivery system: An overview," J. Adv. Pharm. Technol. Res., vol. 1, no. 4, pp. 381-387, 2010. doi: 10.4103/0110-5558.76436.

[15] S. Le Guellec, S. Ehrmann, and L. Vecellio, "In vitro - in vivo correlation of intranasal drug deposition," Adv. Drug Deliv. Rev., vol. 170, pp. 340-352, 2021. doi: 10.1016/j.addr.2020.09.002.

[16] S. S. Sangolkar, V. S. Adhao, D. G. Mundhe, et al., "Particle size determination of nasal drug delivery system: A review," J. Drug Deliv. Ther., vol. 17, pp. 66-73, Nov. 2012.

[17] F. Yang et al., "The effects of surface morphology on the aerosol performance of spray-dried particles within HFA 134a based metered dose formulations," Asian Journal of Pharmaceutical Sciences, vol. 10, no. 6, pp. 513-519, 2015. doi: 10.1016/j.ajps.2015.07.006.

[18] F. Buttini et al., "The application of Quality by Design framework in the pharmaceutical development of dry powder inhalers," Eur J Pharm Sci, vol. 113, pp. 64-76, Feb. 15, 2018. doi: 10.1016/j.ejps.2017.10.042. PMID: 29104067.

[19] L. T. Fasiolo et al., "Opportunity and challenges of nasal powders: Drug formulation and delivery," Eur J Pharm Sci, vol. 113, pp. 2-17, 2018. doi: 10.1016/j.ejps.2017.09.027.

[20] H. Kublik and M. T. Vidgren, "Nasal delivery systems and their effect on deposition and absorption," Adv Drug Deliv Rev, vol. 29, no. 1-2, pp. 157-177, 1998. doi: 10.1016/S0169-409X(97)00067-7.

[21] H. Willden, "Adult Nasal High Flow Therapy: Informed and Educated," American Association for Respiratory Care. [Online]. Available: https://www.aarc.org/nn19-nasal-high-flow-therapy/. [Accessed: 21 March, 2023].

[22] T. A. Willemsz et al., "Kinetic energy density and agglomerate abrasion rate during blending of agglomerates into powders," Eur. J. Pharm. Sci., vol. 45, no. 1-2, pp. 211-215, Jan. 2012. doi: 10.1016/j.ejps.2011.11.012. PMID: 22127372.

[23] M. Chaturvedi, M. Kumar, and K. Pathak, "A review on mucoadhesive polymer used in nasal drug delivery system," J. Adv. Pharm. Technol. Res., vol. 2, no. 4, pp. 215-222, Oct. 2011. doi: 10.4103/2231-4040.90876. PMID: 22247888; PMCID: PMC3255357.

[24] L. Illum, A.N. Fisher, I. Jabbal-Gill, and S.S. Davis, "Bioadhesive starch microspheres and absorption enhancing agents act synergistically to enhance the nasal absorption of polypeptides," Int. J. Pharm., vol. 222, no. 1, pp. 109-119, Jul. 2001. doi: 10.1016/s0378-5173(01)00708-6. PMID: 11404037.

[25] L. Kumar, S. Verma, B. Vaidya, and V. Gupta, "Chapter 10 - Bioadhesive Polymers for Targeted Drug Delivery," in V. Mishra, P. Kesharwani, M.C.I. Mohd Amin, and A. Iyer, Eds., Nanotechnology-Based Approaches for Targeting and Delivery of Drugs and Genes, Academic Press, 2017, pp. 322-362, ISBN: 9780128097175. doi: 10.1016/B978-0-12-809717-5.00012-9. Available: https://www.sciencedirect.com/science/article/pii/B9780128097175000129.

[26] M. Jiménez-Castellanos, H. Zia, and C. Rhodes, "Mucoadhesive Drug Delivery Systems," Drug Dev Ind Pharm, vol. 19, pp. 143-194, Oct. 2008. doi: 10.3109/03639049309038765.

[27] A. V. Yadav and H. H. Mote, "Development of biodegradable starch microspheres for intranasal delivery," Indian J Pharm Sci, vol. 70, no. 2, pp. 170-174, 2008. doi: 10.4103/0250-474X.41450.

[28] I. C. Thaarup, C. Gummesson, and T. Bjarnsholt, "Measuring enzymatic degradation of degradable starch microspheres using confocal laser scanning microscopy," Acta Biomater, vol. 131, pp. 464-471, Sep. 2021. doi: 10.1016/j.actbio.2021.06.042. PMID: 34214664.

[29] S. Mansuri, P. Kesharwani, K. Jain, R. K. Tekade, and N. K. Jain, "Mucoadhesion: A promising approach in drug delivery system," Reactive and Functional Polymers, vol. 100, pp. 151-172, 2016. ISSN 1381-5148. doi: 10.1016/j.reactfunctpolym.2016.01.011.
[30] Purdue University, "Scanning Electron Microscope," Purdue University, [Online]. Available:https://www.purdue.edu/ehps/rem/laboratory/equipment%20safety/Research%20Equipment/sem.html. [Accessed: 02-May-2023].

[31] "Scanning electron microscopy principles," Thermo fisher Scientific, [Online]. Available: https://www.thermofisher.com/se/en/home/materials-science/learning-center/applications/scanning-electron-microscope-sem-electron-column.html. [Accessed: 02-May-2023].

[32] P. Surkar, "Measurement of Particle Size Distribution (PSD) by Laser Diffraction Technique," LinkedIn, 15-Apr-2023. [Online]. Available: https://www.linkedin.com/pulse/measurement-particle-size-distribution-psd-laser-technique-surkar/. [Accessed: 02-May-2023].

[33] "What is the Gravimetric Sorption Technique?," HIDEN isochema, Mar. 15, 2018. [Online]. Available: https://hidenisochema.com/news-press/what-is-the-gravimetric-sorption-technique/. [Accessed: 02-May-2023].

[34] "BET Specific Surface Area," Particletechlabs. [Online]. Available: https://particletechlabs.com/analytical-testing/bet-specific-surface-area/. [Accessed: 03-May-2023].

[35] "Gas adsorption: Determination of the specific surface area (BET surface area)," 3P Instruments GmbH & Co. KG. [Online]. Available: https://www.3p-instruments.com/measurement-methods/bet-surface-area/. [Accessed: 03-May-2023].

[36] "Gas Pycnometers: True Density Analysis of Powders, Foams and Bulk Solids," Quantachrome Corporation, Boynton Beach, FL, USA, 2019. [Online]. Available: https://dlu.com.ua/Files/ProductLine/Gas_Pycnometers_Brochure.pdf.

[37] "Spraytec," Malvern Panalytical. [Online]. Available: https://www.malvernpanalytical.com/en/products/product-range/spraytec.

7 Appendix

7.1 Appendix A

Tables 7.1-7.4 contains raw data for DSM-A, DSM-S, DSM-T and DSM-L obtained from PSD analysis in suspension for each setting.

Table 7.1: Displays the different parameters generated from PSD analysis in suspension of DSM-A.

Sample	d10 (µm)	d50 (µm)	d90 (µm)	Above 100 µm (%)	Below 10 µm (%)	Specific surface area (m2/kg)	Span
Stirrer 1 min	31.2	52.8	85.1	3.6	1.7	127.3	1.0
Stirrer 1 min, 20% sonication	31.2	52.3	83.3	2.7	1.8	132.2	1.0
Stirrer 3 min, 60% sonication	31.0	51.9	82.4	2.3	1.8	132.7	1.0

Table 7.2: Presents the results of PSD analysis conducted in suspension of DSM-S, displaying the values of various parameters obtained.

Sample name	d10 (µm)	d50 (µm)	d90 (µm)	Above 100 µm (%)	Below 10 µm (%)	Specific surface area (m2/kg)	Span
Stirrer 1 min	15.9	28.0	114.0	11.1	1.7	222.7	3.5
Stirrer 1 min, 20% sonication	15.1	24.5	44.6	3.2	2.2	264.3	1.2
Stirrer 3 min, 60% sonication	15.4	23.5	35.3	0.0	2.4	280.1	0.8

Table 7.3: Shows the results of the PSD analysis performed on a suspension of DSM-T. The generated values of the different parameters obtained are presented.

Sample name	d10 (µm)	d50 (µm)	d90 (µm)	Above 100 µm (%)	Below 10 µm (%)	Specific surface area (m2/kg)	Span
Stirrer 1 min	17.3	26.5	41.3	2.3	3.1	279.5	0.9
Stirrer 1 min, 20% sonication	18.2	25.0	33.5	0.0	3.4	298.7	0.6
Stirrer 3 min, 60% sonication	18.4	24.9	32.9	0.0	23.4	300.0	0.6

Table 7.4: Displays the values obtained for different parameters from the PSD analysis carried out on a suspension of DSM-L.

Sample name	d10 (µm)	d50 (µm)	d90 (µm)	Above 100 µm (%)	Below 10 µm (%)	Specific surface area (m2/kg)	Span
Stirrer 1 min	83.5	170	311.0	82.5	0.0	27.4	1.3
Stirrer 1 min, 20% sonication	67.2	96.1	138.0	44.6	0.0	43.2	0.7
Stirrer 3 min, 60% sonication	65.3	90.1	124.0	34.2	0.0	45.8	0.6

Tables 7.5-7.8 displays the generated values at different pressure settings from PSD analysis using the dry powder method for DSM-A stored under various RH levels of dry, 53% RH, 75% RH and 94% RH.

Table 7.5. The generated values of the different parameters for DSM-A stored under dry conditions

Pressure (Bar)	Dx (10) (µm)	Dx (50) (µm)	Dx (90) (µm)	Above 100 µm (%)	Below 10 µm (%)	Specific surface area (m2/kg)	Span
0.3	39.8	58.7	86.2	3.3	0.0	71.2	0.2
1	36.5	56.0	84.7	2.9	0.0	75.3	0.3
3	33.9	55.1	87.4	4.3	0.0	77.9	0.3

Table 7.6. The generated values of the different parameters for DSM-A stored under RH 53%.

Pressure (Bar)	Dx (10) (µm)	Dx (50) (µm)	Dx (90) (µm)	Above 100 µm (%)	Below 10 µm (%)	Specific surface area (m2/kg)	Span
0.3	33.2	55.3	89.0	4.9	0.4	80.1	1.0
1	32.4	53.8	86.2	4.0	0.4	82.1	1.0
3	32.1	53.5	86.1	4.0	0.0	81.0	1.0

Table 7.7. The generated values of the different parameters for DSM-A stored under RH 75%.

Pressure (Bar)	Dx (10) (µm)	Dx (50) (µm)	Dx (90) (µm)	Above 100 µm (%)	Below 10 µm (%)	Specific surface area (m2/kg)	Span
0.3	36.0	58.5	94.7	7.5	0.3	74.2	1.0
1	35.4	57.1	91.7	6.2	0.3	76.0	1.0
3	35.1	56.9	91.6	6.2	0.4	76.6	1.0

Table 7.8. The generated values of the different parameters for DSM-A stored under RH 94%.

Pressure (Bar)	Dx (10) (µm)	Dx (50) (µm)	Dx (90) (µm)	Above 100 µm (%)	Below 10 µm (%)	Specific surface area (m2/kg)	Span
0.3	38.4	80.4	1880.0	40.7	0.2	50.8	22.9
1	36.5	74.1	1880.0	37.4	0.2	54.0	24.8
3	34.2	62.2	1120.0	23.8	0.3	66.0	17.4

Tables 7.9-7.12 displays the generated values at different pressure settings from PSD analysis using the dry powder method for DSM-S stored under various RH levels of dry, 53% RH, 75% RH and 94% RH.

Table 7.9. The generated values of the different parameters for DSM-S stored under dry conditions.

Pressure (Bar)	Dx (10) (µm)	Dx (50) (µm)	Dx (90) (µm)	Above 100 µm (%)	Below 10 µm (%)	Specific surface area (m2/kg)	Span
0.3	15.2	26.4	535	17.1	1.7	381.7	19.7
1	16.6	24.4	40.5	7.1	0.0	163.7	1.0
3	16.6	23.2	34.4	5.1	0.0	172.5	0.8

Table 7.10. The generated values of the different parameters for DSM-s stored under RH 53%.

Pressure (Bar)	Dx (10) (µm)	Dx (50) (µm)	Dx (90) (µm)	Above 100 µm (%)	Below 10 µm (%)	Specific surface area (m2/kg)	Span
0.3	16.2	26.2	164.0	3.1	0.0	150.2	5.6
1	16.7	24.8	48.8	8.7	0.0	160.0	1.3
3	16.7	24.0	38.3	6.8	0.0	166.1	0.9

Table 7.11. The generated values of the different parameters for DSM-S stored under RH 75%.

Pressure (Bar)	Dx (10) (µm)	Dx (50) (µm)	Dx (90) (µm)	Above 100 µm (%)	Below 10 µm (%)	Specific surface area (m2/kg)	Span
0.3	16.3	27.0	406.0	15.8	0.0	144.5	14.5
1	16.8	24.9	47.8	8.45	0.0	159.1	1.2
3	16.5	24.1	39.1	6.4	0.0	166.3	0.9

Table 7.12. The generated values of the different parameters for DSM-S stored under RH 94%.

Pressure (Bar)	Dx (10) (µm)	Dx (50) (µm)	Dx (90) (µm)	Above 100 µm (%)	Below 10 µm (%)	Specific surface area (m2/kg)	Span
0.3	16.6	28.0	874.0	19.9	0.0	137.1	30.7
1	16.8	25.4	112.0	10.7	0.0	154.7	3.7
3	16.6	24.3	40.7	7.3	0.0	164.0	1.0

7.2 Appendix B

Tables 7.13-7.16 in this section present the raw data obtained from bulk density measurements, including the calculated masses for each of the three measurements. These tables display the calculated mean weight value from the three measurements, the corresponding standard deviation value, and the calculated bulk density.

Table 7.13. The calculated mass from three measurements, the mean mass value and the corresponding standard deviation value, including the bulk density value for DSM-A.

Experiment	Mass (g)	Mean mass value (g)	Standard Deviation	Bulk density (g/cm^3)
1	2.74	2.75	0.01	0.53
2	2.76			
3	2.75			

Table 7.14. The calculated mass from three measurements, the mean mass value and the corresponding standard deviation value, including the bulk density value for DSM-S.

Experiment	Mass (g)	Mean mass value (g)	Standard Deviation	Bulk density (g/cm^3)
1	3.15	3.13	0.02	0.60
2	3.10			
3	3.15			

Table 7.15. The calculated mass from three measurements, the mean mass value and the corresponding standard deviation value, including the bulk density value for DSM-T.

Experiment	Mass (g)	Mean mass value (g)	Standard Deviation	Bulk density (g/cm^3)
1	3.48	3.47	0.01	0.67
2	3.47			
3	3.46			

Table 7.16. The calculated mass from three measurements, the mean mass value and the corresponding standard deviation value, including the bulk density value for DSM-L.

Experiment	Mass (g)	Mean mass value (g)	Standard Deviation	Bulk density (g/cm^3)
1	3.08	3.09	0.01	0.59
2	3.09			
3	3.11			

7.3 Appendix C

Table 7.17 displays the generated weight for each sample, while Table 7.18 presents the raw data obtained from the pycnometer experiment used to calculate the true density value shown in Table 7.19.

Table 7.17. The calculated weights for each DSM batch.

Sample	Mass (g)
DSM-T	0.55
DSM-L	0.47
DSM-S	0.56
DSM-A	0.45

Table 7.18. The generated average volume for each DSM batch from the pycnometer experiment.

Sample	Volume (cm^3)
DSM-T	0.42
DSM-L	0.36
DSM-S	0.42
DSM-A	**0.37**

Table 7.19. The calculated true density for each DSM batch.

Sample	True density (g/cm^3)
DSM-T	1.32
DSM-L	1.30
DSM-S	1.32
DSM-A	1.22

7.4 Appendix D

The tables below present the height of the piles formed by the different DSM batches, including Nasaleze, which were stored under various RH levels. The measurements were obtained from the angle of repose experiments and this raw data was utilized to calculate the angle of repose, which serves as an indicator of flowability.

Table 7.20. The determined height of the pile of DSM-A, stored under dry conditions, with the funnel placed at setting 0 cm on the instrument.

Experiment	Height (mm)
1	4.15
2	4.68
3	4.04
4	4.38
5	4.23

Table 7.21. The determined height of the pile of DSM-A, stored at 53% RH, with the funnel placed at setting 0 cm on the instrument.

Experiment	Height (mm)
1	6.19
2	5.58
3	5.56
4	5.11

Table 7.22. The determined height of the pile of DSM-A, stored at 75% RH, with the funnel placed at setting 1 cm on the instrument.

Experiment	Height (mm)
1	10.93
2	10.92
3	10.44
4	8.68

Table 7.23. The determined height of the pile of DSM-S, stored under dry conditions, manually added.

Experiment	Height (mm)
1	7.93
2	11.27
3	9.38
4	9.74
5	10.78
6	8.64

Table 7.24. The determined height of the pile of DSM-S, stored at 53% RH, with the funnel placed at setting 0 cm on the instrument.

Experiment	Height (mm)
1	12.78
2	17.55
3	15.73
4	14.18
5	13.42
6	13.39
7	13.93

Table 7.25. The determined height of the pile of DSM-S, stored at 75% RH, with the funnel placed at setting 0 cm on the instrument.

Experiment	Height (mm)
1	17.10
2	18.47
3	17.43
4	15.29
5	16.22

Table 7.26. The determined height of the pile of DSM-T, stored under dry conditions, with the funnel placed at setting 0 cm on the instrument.

Experiment	Height (mm)
1	11.82
2	6.18
3	5.78
4	6.00
5	6.62
6	6.90
7	7.18
8	6.64

Table 7.27. The determined height of the pile of DSM-L, stored under dry conditions, with the funnel placed at setting 0 cm on the instrument.

Experiment	Height (mm)
1	6.68
2	7.06
3	6.94
4	6.55
5	7.14
6	6.83
7	6.68

7.5 Appendix E

Tables 7.28-7.32 display the raw data obtained from the GVS experiment for each DSM batch and Nasaleze, presenting the sorption value, desorption value, and hysteresis value at the various RH levels for one cycle.

Table 7.28. The generated sorption value, desorption value, and hysteresis value at the various RH levels for DSM-A.

Target	Change In Mass (%) - ref		
% P/Po	Sorption	Desorption	Hysteresis
0.0		0.01	
20.0	9.72	8.05	-1.67
30.0	11.45		
40.0	12.83	12.39	-0.44
50.0	14.27		
60.0	15.61	16.93	1.32
70.0	17.64		
80.0	20.83	20,.83	

Table 7.29. The generated sorption value, desorption value, and hysteresis value at the various RH levels for DSM-S

Target	Change In Mass (%) - ref		
% P/Po	Sorption	Desorption	Hysteresis
0,0		0.01	
20.0	8.62	8.24	-0.39
30.0	9.66		
40.0	11.70	12.62	0.92
50.0	13.84		
60.0	15.60	17.23	1.62
70.0	17.88		
80.0	21.04	21.04	

Table 7.30. The generated sorption value, desorption value, and hysteresis value at the various RH levels for DSM-T.

Target	Change In Mass (%) - ref		
% P/Po	Sorption	Desorption	Hysteresis
0.0		0.01	
20.0	9.66	8.31	-1.35
30.0	10.89		
40.0	12.14	12.97	0.83
50.0	14.06		
60.0	16.04	17.51	1.47
70.0	18.52		
80.0	22.05	22.05	

Table 7.31. The generated sorption value, desorption value, and hysteresis value at the various RH levels for DSM-L.

Target	Change In Mass (%) - ref		
% P/Po	Sorption	Desorption	Hysteresis
0.0		0.01	
20.0	8.61	7.13	-1.47
30.0	10.21		
40.0	11.78	11.57	-0.21
50.0	13.98		
60.0	15.68	16.27	0.60
70.0	17.43		
80.0	20.21	20.21	

Table 7.32. The generated sorption value, desorption value, and hysteresis value at the various RH levels for Nasaleze.

Target	Change In Mass (%) - ref		
% P/Po	Sorption	Desorption	Hysteresis
0.0		0.00	
20.0	3.25	3.36	0.11
30.0	4.42		
40.0	5.62	6.59	0.97
50.0	7.05		
60.0	8.75	11.06	2.30
70.0	12.13		
80.0	16.46	16.46	

7.6 Appendix F

Table 7.33 -7.38 displays the fill weight of the different DSM batches in activity of the ICOone Nasal delivery device. The calculated retention for each dose and the corresponding standard deviation is also present.

Table 7.33. The fill weight of the DSM-A sample in the cavity of the ICOone Nasal, along with the calculated retention value obtained from the ICOone delivery device. The retention values are provided for DSM-A stored under different RH levels, accompanied by the corresponding standard deviation value.

Sample	Storage condition	Fill weight (mg)	Retention (%)	Standarddeviation
DSM-A	Dry	24.1	0.00	6.57
DSM-A	Dry	17.3	0.00	
DMS-A	Dry	21.1	11.37	
DSM-A	53% RH	26.8	4.48	2.02
DSM-A	53% RH	25.5	0.39	
DSM-A	75% RH	27.6	1.45	41.68
DSM-A	75% RH	22.1	0.00	
DSM-A	75% RH	31.0	72.90	

Table 7.34. The fill weight of the DSM-S sample in the cavity of the ICOone Nasal device, along with the calculated retention value obtained from the ICOone delivery device. The retention values are provided for DSM-S stored under different RH levels, accompanied by the corresponding standard deviation value.

Sample	Storage condition	Fill weight (mg)	Retention (%)	Standarddeviation
DSM-S	Dry	16.4	40.24	2.35
DSM-S	Dry	18.8	42.02	
DSM-S	Dry	18.2	37.36	
DSM-S	53% RH	40.1	0.00	3.22
DSM-S	53% RH	29.4	6.80	
DSM-S	53% RH	35.0	0.00	
DSM-S	75% RH	37.4	62.57	32.68
DSM-S	75% RH	49.8	5.42	
DSM-S	75% RH	32.2	6.52	

Table 7.35. The fill weight of the DSM-T sample in the cavity of the ICOone Nasal device, along with the calculated retention value obtained from the ICOone delivery device. The retention values are provided for DSM-T stored under different RH levels, accompanied by the corresponding standard deviation value.

Sample	Storage condition	Fill weight (mg)	Retention (%)	Standarddeviation
DSM-T	Dry	18.3	7.65	22.14
DSM-T	Dry	12.8	38.28	
DSM-T	Dry	15.0	50.67	
DSM-T	53% RH	39.1	2.81	1.99
DSM-T	53% RH	39.4	0.00	
DSM-T	75% RH	48.7	65.30	28.69
DSM-T	75% RH	32	74.06	
DSM-T	75% RH	35	20.57	

Table 7.36. The fill weight of the DSM-L sample in the cavity of the ICOone Nasal device, along with the calculated retention value obtained from the ICOone delivery device. The retention values are provided for DSM-L stored under different RH levels, accompanied by the corresponding standard deviation value.

Sample	Storage condition	Fill weight (mg)	Retention (%)	Standarddeviation
DSM-L	Dry	12.6	30.16	12.86
DSM-L	Dry	19.5	0.76	
DSM-L	Dry	16.0	0.74	
DSM-L	53% RH	47.2	5.93	6.00
DSM-L	53% RH	46.8	13.46	
DSM-L	53% RH	37.6	1.60	
DSM-L	75% RH	40.6	0.00	2.14
DSM-L	75% RH	43.2	3.70	
DSM-L	75% RH	22.2	0.00	

Table 7.37. The fill weight of the Nasaleze in the cavity of the ICOone Nasal device, along with the calculated retention value obtained from the ICOone delivery device. The retention values are provided for Nasaleze stored under Dry conditions, accompanied by the corresponding standard deviation value.

Sample	Storage condition	Fill weight (mg)	Retention (%)	Standarddeviation
Nasaleze	Dry	54.4	8.09	2.29
Nasaleze	Dry	54.1	5.73	
Nasaleze	Dry	65.3	3.52	
Nasaleze	Dry	57,7	1.21	
Nasaleze	Dry	59	5.08	

Table 7.38. Calculated retention and the corresponding standard deviation value of the DSM-A and DSM-S batches analyzed at 40 and 20 L/min flow rates.

Sample	Flow rate (L/min)	Retention (%)	Standarddeviation
DSM-A	40	0	0.01
DSM-A	40	2	
DSM-A	40	1.7	
DSM-A	20	21	0.15
DSM-A	20	13	
DSM-A	20	48	
DSM-S	40	2	0.11
DSM-S	40	26	
DSM-S	40	3	
DSM-S	20	20	0.26
DSM-S	20	76	
DSM-S	20	74	